INVESTIGATION OF ATMOSPHERIC OZONE IMPACTS OF 2,3,3,3-TETRAFLUOROPROPENE

Final Report to the

Honeywell International Inc
Contract UCR-09010016

By

William P. L. Carter

June 2, 2009

Center for Environmental Research and Technology
College of Engineering
University of California
Riverside, California 92521

ABSTRACT

An experimental and modeling study was carried out to assess the impacts of 2,3,3,3-tetrafluoropropene on ground-level ozone formation compared to other chemicals that are emitted into the atmosphere. The experiments consisted of incremental reactivity environmental chamber experiments to determine the effect of adding the tetrafluoropropene to irradiations of reactive organic gas (ROG) surrogate - NO_x mixtures representing ambient conditions. The results were modeled using the SAPRC-07 mechanism with the reactions of the tetrafluoropropene added. The data were reasonably well simulated if it is assumed that nitrate formation from the reactions of peroxy radicals with NO was negligible. This mechanism was then used to calculate the atmospheric impact of the tetrafluoropropene in the box model scenarios to derive the Maximum Incremental Reactivity (MIR) and other ozone reactivity scales. 2,3,3,3-Tetrafluoropropene was calculated to have an ozone impact on a mass basis that is the same as that of ethane to within the variability of the model for atmospheric conditions. The average ratio of mass-based incremental reactivities relative to ethane was 0.9±0.2 and the MIR ratio was 1.0±0.1. It is concluded that if ethane is used as the standard to define "negligible" ozone impact for the purpose of determining VOC exemptions for ozone precursors, then 2,3,3,3-tetrafluoropropene might meet this standard. 2,3,3,3-Tetrafluoropropene was also found to have no significant effect on particle formation in the incremental reactivity chamber experiments.

ACKNOWLEDGEMENTS AND DISCLAIMERS

This work was funded by Honeywell International Inc. through contract UCR-09010016. The environmental chamber experiments for this project were carried out at the College of Engineering Center for Environmental Research and Technology (CE-CERT) primarily by Qi Li, Kurt Bumiller, and Quentin Malloy. Mr. Dennis Fitz also provided assistance in administering this project, and Ms. Kathy Cocker provided assistance in conducting the experiments and processing the data.

Although Honeywell International Inc. funded this work, the contents of this report reflect only the opinions and conclusions of the author. Mention of trade names and commercial products does not constitute endorsement or recommendation for use.

TABLE OF CONTENTS

LIST OF TABLES

LIST OF FIGURES

INTRODUCTION

Ozone in photochemical smog is formed from the gas-phase reactions of volatile organic compounds (VOCs) and oxides of nitrogen (NO_x) in sunlight, and control of both VOCs and NO_x is required to attain air quality standards for ozone. Many different types of VOCs are emitted into the atmosphere, each reacting at different rates and having different mechanisms for their reactions. Because of this, they can differ significantly in their effects on ozone formation, or their "reactivity". In recognition of this, the U.S. EPA has exempted volatile organic certain compounds with ozone impacts expected to be less than ethane from regulations as VOC ozone precursors (Dimitriades, 1999; RRWG, 1999a, EPA, 2005), and the California Air Resources Board (CARB) has adopted regulations with reactivity-based adjustments for several types of VOC sources (CARB 1993, 2000) and is investigating their use for other sources (CARB, 2008).

Fluorinated propenes such as 2,3,3,3-tetrafluoropropene ($CF_3CF=CH_2$) are compounds of interest to Honeywell Specialty Materials Company whose use and manufacture may result in their being emitted into the atmosphere. This will result in these compounds being subject to VOC regulations aimed at reducing ozone formation, which may adversely impact their production costs and marketability. If these compounds can be shown to have ozone impacts less than or equal to ethane on a mass basis, a case might be made to the U.S. EPA to exempt them from regulations as VOC ozone precursors (EPA, 2005). Because of this, Honeywell contracted us to develop estimates of ozone impacts of these compounds in various ozone reactivity scales, and compare them with the ozone impacts for ethane (Carter, 2009a).

The results of our assessment indicated that 2,3,3,3-tetrafluoropropene has about the same ozone impact as ethane on a mass basis (Carter, 2008). However, the ability of mechanisms to predict ozone impacts had not been experimentally verified for this compound, and an experimental study is required to support the use of these reactivity values in a petition to the EPA to exempt this compound from regulations on the basis of relatively low reactivity for ozone formation.

In view of this, Honeywell Corporation funded the College of Engineering, Center for Environmental Research and Technology (CE-CERT) at the University of California at Riverside (UCR) to carry out a project to reduce uncertainties in estimates of the atmospheric ozone impacts of 2,3,3,3-tetrafluoropropene. This included conducting environmental chamber experiments suitable for testing mechanisms for the gas-phase atmospheric reactions of this compound that affect ozone formation, using the results to evaluate the mechanism previously derived for this compound, revising or adjusting the mechanism to simulate the data, and recalculating its atmospheric impacts if the mechanism is revised. The approach used is similar to that used many other VOCs that have been studied previously (Carter, 2009a, and references therein), including the fluorinated propene trans 1,3,3,3-tetrafluoropropene that was studied previously for Honeywell (Carter, 2009b). The methods, results, and conclusions of this project are documented in this report.

EXPERIMENTAL METHODS

Chamber Description

All of the environmental chamber experiments for this project were carried out using the UCR EPA environmental chamber at CE-CERT. This is the same as the chamber used in our recently completed study of trans 1,3,3,3-tetrafluoropropene (Carter, 2009b). This chamber was constructed under EPA funding to address the needs for an improved environmental chamber database for mechanism evaluation (Carter et al, 1999, Carter, 2002). The objectives, design, construction, and results of the initial evaluation of this chamber facility are described in more detail elsewhere (Carter et al, 1999, Carter, 2002; Carter, 2004, Carter et al, 2005a). A brief description of the chamber is also given below.

The UCR EPA chamber consists of two ~85,000-liter Teflon® reactors located inside a 16,000 cubic ft temperature-controlled "clean room" that is continuously flushed with purified air. The clean room design is employed in order to minimize background contaminants into the reactor due to permeation or leaks. Two alternative light sources can be used. The first consists of a 200 KW argon arc lamp with specially designed UV filters that give a UV and visible spectrum similar to sunlight. Banks of blacklights are also present to serve as an alternative lower cost light source when blacklight irradiation is sufficient. Blacklights have a good representation of sunlight in the UV portion of the spectrum that affects most photolysis reactions of interest, and their use is sufficient for test compounds whose mechanisms involve do not involve photoreactive compounds, or only photoreactive compounds with known action spectra (Carter et al, 1995b). Since this is the case for the fluoropropenes studied here and by Carter (2009b), they were used for all experiments for this project. The interior of the enclosure is covered with reflective aluminum panels in order to maximize the available light intensity and to attain sufficient light uniformity, which is estimated to be ±10% or better in the portion of the enclosure where the reactors are located (Carter, 2002). A diagram of the enclosure and reactors is shown in Figure 1, and spectra of the light sources are shown in Figure 2.

The dual reactors are constructed of flexible 2 mil Teflon® film, which is the same material used in the other UCR Teflon chambers used for mechanism evaluation (e.g., Carter et al, 1995a; Carter, 2000a, and references therein). A semi-flexible framework design was developed to minimize leakage and simplify the management of large volume reactors. The Teflon film is heat-sealed into separate sheets for the top, bottom, and sides (the latter sealed into a cylindrical shape) that are held together and in place using bottom frames attached to the floor and moveable top frames. The moveable top frame is held to the ceiling by cables that are controlled by motors that raise the top to allow the reactors to expand when filled or lower the top to allow the volume to contract when the reactors are being emptied or flushed. These motors in turn are controlled by pressure sensors that raise or lower the reactors as needed to maintain slight positive pressure. During experiments the top frames are slowly lowered to maintain continuous positive pressure as the reactor volumes decrease due to sampling or leaks. The experiment is terminated once the volume of one of the reactor reaches about 1/3 the maximum value, where the time this took varied depending on the amount of leaks in the reactor, but was greater than the duration of most of the experiments discussed in this report. Since at least some leaks are unavoidable in large Teflon film reactors, the constant positive pressure is important to minimize the introduction of enclosure air into the reactor that may otherwise result.

As indicated in Figure 1, the floor of the reactors has openings for a high volume mixing system for mixing reactants within a reactor and also for exchanging reactants between the reactors to achieve

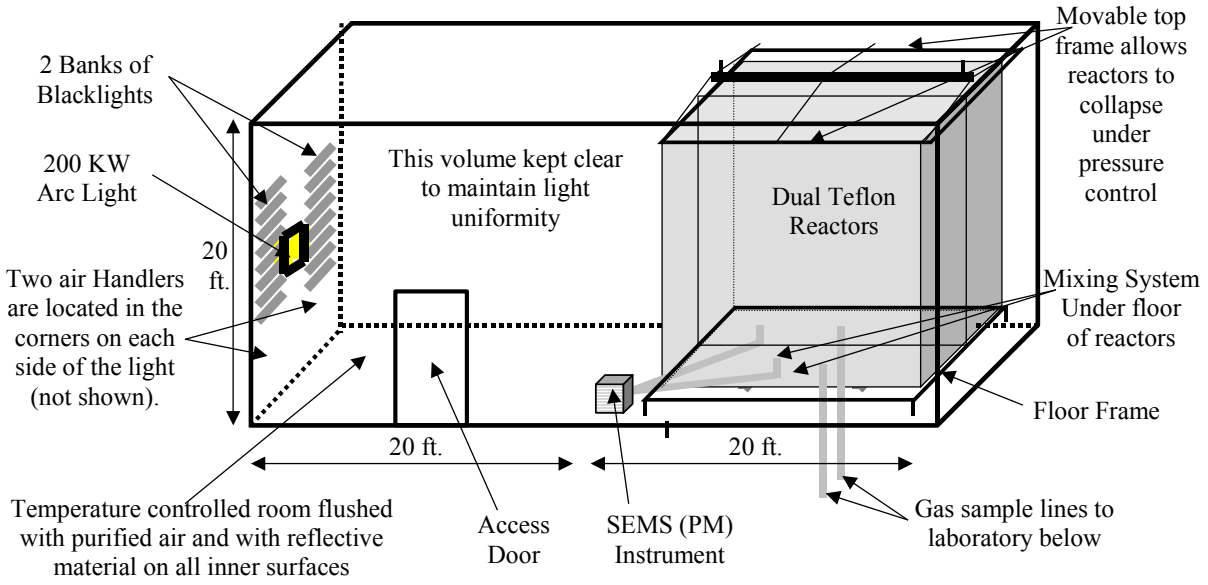

Figure 1. Schematic of the UCR EPA environmental chamber reactors and enclosure.

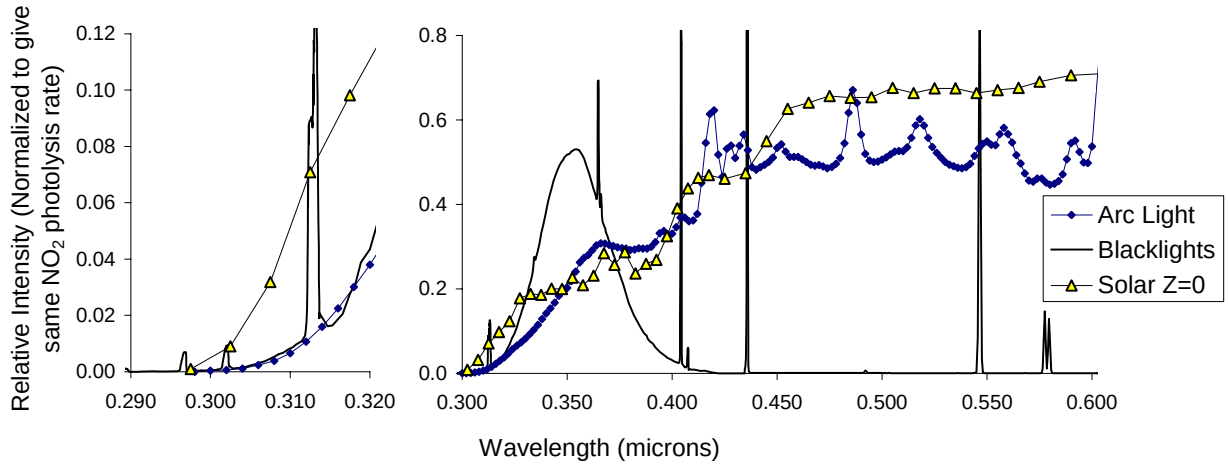

Figure 2. Spectrum of the light sources used in the UCR EPA chamber, with intensities normalized to give the same NO_2 photolysis rates. A representative solar spectrum is also shown.

equal concentrations in each. This utilizes four 10" Teflon pipes with Teflon-coated blowers and flanges to either blow air from one side of a reactor to the other, or to move air between each of the two reactors. Teflon-coated air-driven metal valves are used to close off the openings to the mixing system when not in use, and during the irradiation experiments.

An AADCO air purification system that provides dry purified air at flow rates up to 1500 liters min^{-1} is used to supply the air to flush the enclosure and to flush and fill the reactors between experiments. The air is further purified by passing it through cartridges filled with Purafil® and heated Carulite 300® which is a Hopcalite® type catalyst and also through a filter to remove particulate matter. The measured NO_x, CO, and non-methane organic concentrations in the purified air were found to be less than the detection limits of the instrumentation employed (see Analytical Equipment, below).

The chamber enclosure is located on the second floor of a two-floor laboratory building that was designed and constructed specifically to house this facility (Carter et al, 2002). Most of the analytical instrumentation is located on the ground floor beneath the chamber, with sampling lines leading down as indicated in Figure 1.

Analytical Instrumentation

Table 1 gives a listing of the analytical and characterization instrumentation whose data were utilized for this project. Other instrumentation was available and used for some of these experiments, as discussed by Carter 2002a and Carter et al, 2005a, but the data obtained were not characterized for modeling and thus not used in the mechanism evaluations for this project. The table includes a brief description of the equipment, species monitored, and their approximate sensitivities, where applicable. These are discussed further in the following sections.

Ozone, CO, NO, and NO_y were monitored using commercially available instruments as indicated in Table 1. The instruments were spanned for NO, NO_2, and CO and zeroed prior to all experiments using the gas calibration system indicated in Table 1, and a prepared calibration gas cylinder with known amounts of NO and CO. O_3 and NO_2 spans were conducted by gas phase titration using the calibrator during this period. Span and zero corrections were made to the NO, NO_2, and CO data as appropriate based on the results of these span measurements, and the O_3 spans indicated that the UV absorption instrument was performing within its specifications.

Organic reactants were measured by gas chromatography with FID detection as described elsewhere (Carter et al, 1995a); see also Table 1. The surrogate gaseous compounds ethylene, propylene, n-butane and trans-2-butene were monitored by using 30 m megabore GS-Alumina column and the loop sampling system. The second signal of the same GC outfitted with FID, loop sampling system and 30 m megabore DB-5 column was used to analyze surrogate liquid components toluene, n-octane and m-xylene. The sampling methods employed for injecting the sample with the test compounds on the GC column depended on the volatility or "stickiness" of the compounds. For analyses of more volatile specie such as 2,3,3,3-tetrafluoropropene the same loop method was suitable.

Both the GC instruments were controlled and their data were analyzed using Agilent ChemStation software installed on a dedicated PC. The GC's were spanned using the prepared calibration cylinder with known amounts of ethylene, propane, propylene, n-butane, n-hexane, toluene, n-octane and m-xylene in ultrapure nitrogen. Analyses of the span mixture were conducted approximately every day an experiment was run, and the results were tracked for consistency.

Table 1. List of analytical and characterization instrumentation for the UCR EPA chamber.

Type	Model or Description	Species	Sensitivity	Comments
Ozone Analyzer	Dasibi Model 1003-AH. UV absorption analysis.	O_3	2 ppb	Standard monitoring instrument.
NO - NO_y Analyzer	Teco Model 42 C with external converter. Chemiluminescent analysis for NO, NOy by catalytic conversion.	NO NO_y	1 ppb 1 ppb	Useful for NO and initial NO_2 monitoring. Converter close-coupled to the reactors so the "NO_y" channel should include HNO_3 as well as NO_2, PANs, organic nitrates, and other species converted to NO by the catalyst.
CO Analyzer	Thermo Environmental Instruments Inc. Model 48 C	CO	50 ppb	Standard monitoring instrument
GC-FID Instruments	Dual Agilent 6890 Series II GC with dual columns, loop injectors and FID detectors. Controlled by computer interfaced to network.	VOCs	~10 ppbC	30 m x 0.53 mm GS-Alumina column used for the analysis of light hydrocarbons such as ethylene, propylene, n-butane and trans-2-butene and 30 m x 0.53 mm DB-5 column used for the analysis of C_{5+} alkanes and aromatics, such as toluene and m-xylene. Loop injection is suitable for low to medium volatility VOCs that are not too "sticky" to pass through valves. Two 30 m x 0.32 mm DB-5 column measure C_{5+} alkanes and aromatics, such as toluene and m-xylene.
Gas Calibrator	Model 146C Thermo Environmental Dynamic Gas Calibrator	N/A	N/A	Used for calibration of NO_x and other analyzers. Instrument acquired early in project and under continuous use.
Data Acquisition Sytem	Windows PC with custom LabView software, 16 analog input, 40 I/O, 16 thermo-couple, and 8 RS-232 channels.	N/A	N/A	Used to collect data from most monitoring instruments and control sampling solenoids. In-house LabView software was developed using software developed by Sonoma Technology for ARB for the Central California Air Quality Study as the starting point.
Temperature sensors	Various thermocouples, radiation shielded thermocouple housing	Tempera-ture	~0.1 ^oC	Primary measurement is thermocouples inside reactor. However, comparison with temperature measurements in the sample line suggest that irradiative heating may bias these data high by ~2.5^oC (Carter, 2004).
Humidity Monitor	General Eastern HYGRO-M1 Dew Point Monitor	Humid-ity	Dew point range: -40 - 50^oC	Instrument performs as expected, but dew point below the performance range for most of the experiments discussed in this report, except for those with added humidity.

Table 1 (continued)

Type	Model or Description	Species	Sensitivity	Comments
Spectro-radiometer	LiCor LI-1800 Spectroradiometer	300-850 nm Light Spect-rum	Adequate	Resolution relatively low but adequate for this project. Used to obtain relative spectrum. Also gives an absolute intensity measurement on surface useful for assessing relative trends.
QSL Spherical Irradiance Sensor	Biospherical QSL-2100 PAR Irradiance Sensor. Responds to 400-700 nm light.	Spherical Broad-band Light Intensity	Adequate	Provides a measure of absolute intensity and light uniformity that is more directly related to photolysis rates than light intensity on surface. Gives more precise measurement of light intensity trends than NO_2 actinometry, but is relatively sensitive to small changes in position.
Scanning Mobility Particle Sizer (SMPS)	TSI 3080L column, TSI 3077 ^{85}Kr neutralizer, and TSI 3771 CPC. Instrument design, control, and operation Similar to that described in Cocker et al. (2001)	Aerosol number and size distribut-ions	Adequate	Provides information on size distribution of aerosols in the 28-735 nm size range, which accounts for most of the aerosol mass formed in our experiments. Data can be used to assess effects of VOCs on secondary PM formation.

The surrogate components analyzed by the above system were calibrated by repeated analysis of a standard mixture containing these compounds, and verified by injecting and sampling known amounts of the compound in calibration chamber of known volume. The amounts of gaseous compounds injected were determined by vacuum methods, using an MKS Baratron precision pressure gauge, and bulbs of known volume, determined by weighing when filled with water. The amounts of liquid compounds injected were determined by measuring amounts injected using microliter syringes. The volumes of the calibration chambers were determined by injecting and analyzing compounds whose analyses have been calibrated previously.

The GC analysis of 2,3,3,3-tetrafluoropropene was calibrated by injecting a quantitative amount of the compound in the chamber reactors. The chamber reactors have a known volume and therefore contain a known concentration of the injected compound. The calibration factor was then determined as a result of the GC analyses conducted prior to the start of the irradiations.

As indicated in Table 1, aerosol number and size distributions were also measured in conjunction with our experiments. The instrumentation employed is similar to that described by Cocker et al. (2001), and is the same as employed in our previous studies of coatings VOCs (Carter et al, 2005b). Particle size distributions are obtained using a scanning mobility particle sizer (SMPS) equipped with a 3077 ^{85}Kr charger, a 3081L cylindrical long column, and a 3771 condensation particle counter (CPC). Flow rates of 2.5 LPM and 0.25 LPM for sheath and aerosol flow, respectively, are maintained using Labview 6.0-assisted PID control of MKS proportional solenoid control valves. Both the sheath and aerosol flow are obtained from the reactor enclosure. The data inversion algorithm described by Collins et al (2002) converts CPC counts versus time to particle size distribution.

Most of the instruments other than the GCs and aerosol instrument were interfaced to a PC-based computer data acquisition system under the control of a LabView program written for this purpose. These data, and the GC data from the Agilent ChemStation computer, were collected over the CE-CERT

computer network and merged into Excel files that are used for applying span, zero, and other corrections, and preparation of the data for modeling.

Sampling methods

Samples for analysis by the continuous monitoring instruments were withdrawn alternately from the two reactors and zero air, under the control of solenoid valves that were in turn controlled by the data acquisition system discussed above. For most experiments the sampling cycle was 5 minutes for each reactor, the zero air, or (for control purposes) the chamber enclosure. The program controlling the sampling sent data to the data acquisition program to indicate which state was being sampled, so the data could be appropriately apportioned when being processed. Data taken less than 3-4 minutes after the sample switched were not used for subsequent data processing. The sampling system employed is described in more detail by Carter (2002).

Samples for GC analysis of surrogate compounds were taken at approximately every 20-minute directly from each of the reactors through the separate sample lines attached to the bottom of the reactors. The GC sample loops were flushed for a desired time with the air from the reactor being sampled.

Characterization Methods

Use of chamber data for mechanism evaluation requires that the conditions of the experiments be adequately characterized. This includes measurements of temperature, humidity, light and wall effects characterization. Wall effects characterization is discussed in detail by Carter (2004) and updated by Carter and Malkina (2005) and Carter (2007) and most of that discussion is applicable to the experiments for this project. The instrumentation used for the other characterization measurements is summarized in Table 1, above, and these measurements are discussed further below.

Temperature was monitored during chamber experiments using calibrated thermocouples attached to thermocouple boards on our computer data acquisition system. The temperature in each of the reactors was continuously measured using relatively fine gauge thermocouples that were located ~1 foot above the floor of the reactors. These thermocouples were not shielded from the light, though it was hoped that irradiative heating would be minimized because of their small size. Experiments where the thermocouple for one of the reactors was relocated to inside the sample line indicated that radiative heating is probably non-negligible, and that a correction needs to be made for this by subtracting ~2.5^{o}C from the readings of the thermocouples in the reactors. This is discussed by Carter (2004).

Light Spectrum and Intensity. The spectrum of the light source in the 300-850 nm region was measured using a LiCor LI-1800 spectroradiometer, which is periodically calibrated at the factory. Spectroradiometer readings were taken periodically, though the relative spectra were found to have very little variation during the course of these experiments. The absolute light intensity is measured by carrying out NO_2 actinometry experiments periodically using the quartz tube method of Zafonte et al (1977) modified as discussed by Carter et al (1995a). In most cases the quartz tube was located in front of the reactors. Since this location is closer to the light than the centers of the reactors, the measurement at this location is expected to be biased high, so the primary utility of these data are to assess potential variation of intensity over time. However, several special actinometry experiments were conducted prior to the experiments carried out for this project where the quartz tube was located inside the reactors, to provide a direct measurement of the NO_2 photolysis rates inside the reactors. The photolysis rates used when modeling these experiments were the same as used by Carter (2009b) when modeling the recently completed experiments for trans 1,3,3,3-tetrafluoropropene.

Experimental Procedures

The reaction bags were collapsed to the minimum volume by lowering the top frames, then cleaned by emptying and refilling them at least six times after each experiment, and then filled with dry purified air on the nights before experiments. Span measurements were generally made on the continuous instruments prior to injecting the reactants for the experiments. The reactants were then injected through Teflon injection lines (that are separate from the sampling lines) leading from the laboratory below to the reactors. The common reactants were injected in both reactors simultaneously, and were mixed by using the reactor-to-reactor exchange blowers and pipes for 10 minutes. The valves to the exchange system were then closed and the other reactants were injected to their respective sides and mixed using the in-reactor mixing blowers and pipes for 1 minute. The contents of the chamber were then monitored for at least 30 minutes prior to irradiation, and samples were taken from each reactor for GC analysis.

Once the initial reactants are injected, stabilized, and sampled, the light or lights employed (argon arc or blacklights) are turned on to begin the irradiation. During the irradiation the contents of the reactors are kept at a constant positive pressure by lowering the top frames as needed, under positive pressure control. The reactor volumes therefore decrease during the course of the experiments, in part due to sample withdrawal and in part due to small leaks in the reactor. A typical irradiation experiment ended after about 6 hours, by which time the reactors are typically down to about half their fully filled volume. Larger leaks are manifested by more rapid decline of reactor volumes, and the run is aborted early if the volume declines to about 1/3 the maximum. This was the case for a few of the experiments discussed in this report. After the irradiation the reactors were emptied and filled six times as indicated above.

The procedures for injecting the various types of reactants were as follows. The NO, and NO_2 were prepared for injection using a vacuum rack. Known pressures of NO, measured with MKS Baratron capacitance manometers, were expanded into Pyrex bulbs with known volumes, which were then filled with nitrogen (for NO) or purified air (for NO_2). In order to maintain constant NO/NO_2 ratios the same two bulbs of specified volume were utilized in most of experiments. The contents of the bulbs were then flushed into the reactor(s) with nitrogen. Some of the gaseous reactants such as propylene (other than for surrogate experiments) and 2,3,3,3-tetrafluoropropene were prepared for injection using a high vacuum rack as well. For experiments with added CO, the CO was purified by passing it through an in-line activated charcoal trap and flushing it into the reactor at a known rate for the amount of time required to obtain the desired concentration. Measured volumes of volatile liquid reactants were injected, using a micro syringe, into a 2 ft long Pyrex injection tube surrounded with heat tape and equipped with one port for the injection of the liquid and other ports to attach bulbs with gas reactants. For injections into both reactors (e.g, the NO_x and base ROG surrogate components in incremental reactivity experiments), one end of the injection tube was attached to the "Y"-shape glass tube (equipped with stopcocks) that was connected to reactors and the other end of injection tube was connected to a nitrogen source. The injections into a single reactor (e.g., for 2,3,3,3-tetrafluoropropene in the reactivity experiments) was similar except the "Y" tube was not used.

The procedures for injection of the hydrocarbon surrogate components were as follows. A cylinder containing n-butane, trans-2-butene, propylene and ethylene in nitrogen, was used for injecting the gaseous components of the surrogate. The cylinder was attached to the injection system and a gas stream was introduced into reactors at controlled flow for certain time to obtain desired concentrations. A prepared liquid mixture with the appropriate ratios of toluene, n-octane and m-xylene was utilized for injection of these surrogate components, using the procedures as discussed above for pure liquid reactants. All the gas and liquid reactants intended to be the same in both reactors were injected at the same time. The injection consisted of opening the stopcocks and flushing the contents of the bulbs and the liquid reactants with nitrogen, with the liquid reactants being heated slightly using heat that surrounded the injection tube. The flushing continued for approximately 10 minutes.

Problems were encountered during the injections of the surrogate components for some of the experiments for this project, resulting from concentrations different from those intended in the experimental design. This is indicated where applicable in the table in the Results section giving the chronological summary of the experiments. Although the initial concentrations were different from those intended, the results were still useful for mechanism testing, and modeling these experiments are included among the results. The primary consequence of these injection problems was a larger number of experiments being conducted with this compound than was initially intended.

The 2,3,3,3-tetrafluoropropene used in these experiments was provided as a gas in a lecture bottle, and was injected into the chamber using vacuum injection methods similar to that discussed above for NO and other gaseous reactants.

Materials

The sources of the NO, CO and the various base case surrogate compounds came from various commercial vendors as employed in previous projects at our laboratory. The 2,3,3,3-tetrafluoropropene, with a stated purity of ≥ 99.9%, was provided by Honeywell. No significant impurities were detected in any of the GC analyses of these samples.

MECHANISM AND MODELING METHODS

Base Mechanism

The starting point for the chemical mechanism evaluated in this work is the SAPRC-07 mechanism as documented by Carter (2009a). This is a complete update of the SAPRC-99 mechanism of Carter (2000a), but it is very similar to it in its major features. The reactions and rate constants in this mechanism are given in tables in Appendix A to this report, and complete documentation of this mechanism is given by Carter (2009a). Files and software implementing this chemical mechanism are available at the SAPRC mechanism web site[1], with the chemical mechanism simulation computer programs available there being essentially the same as those employed in this work.

As discussed previously (Carter, 2000a,b, 2009a), the current SAPRC mechanisms consists of a "base mechanism" that represents the reactions of the inorganic species and common organic products and lumped organic radical model species and "operators", and separate mechanisms for the initial reactions of the many types other organic compounds that are not in the base mechanism. The compounds, or groups of compounds, that are not included in the base mechanism but for which mechanism assignments have been made, are referred to as detailed model species. The latter include all the base ROG surrogate constituents and compounds whose reactivities are being assessed (2,3,3,3-tetrafluoropropene in this case). These compounds can either be represented explicitly, with separate model species with individual reactions or sets of reactions for each, or using lumped model species similar to those employed in the "fixed parameter" version of SAPRC (Carter, 2000b, 2009a). The latter approach is used when modeling complex mixtures in ambient simulations or simulations of experiments with complex mixtures, but the other approach, representing each compound explicitly, is more appropriate when evaluating mechanisms for individual compounds or simple mixtures. This is because the purpose of mechanism evaluations against chamber data is to assess the performance of the mechanism itself, not to assess the performance lumping approaches. The latter is most appropriately assessed by comparing simulations of explicit and condensed versions of the same mechanism in ambient simulations.

In this work, all of the organic constituents in the environmental chamber experiments were represented explicitly using separate model species for each compound, while complex mixture of emitted species in the atmospheric reactivity simulations were represented using the appropriate lumped model species for the fixed parameter mechanism, as indicted in Table A-1 in Appendix A. The reactions and rate constants in the base mechanism are given in Table A-2, and the photolysis rates used are given in Table A-3. These photolysis rates were calculated from applicable actinic flux or light source characterization data and absorption cross-sections and quantum yields given by Carter (2009a).

The version of the SAPRC-07 mechanism used in this work incorporated several corrections relative to the version used in our study of trans 1,3,3,3-tetrafluoropropene (Carter, 2009b), as discussed in Appendix E of Carter (2009a). The relevant corrections primarily concern hydroperoxide reactions that are not important in affecting ozone formation and have no significant affect calculations of ozone impacts of these tetrafluoropropenes.

[1] Reports and files concerning the latest version of the SAPRC chemical mechanisms and their associated reactivity scales are available at http://www.cert.ucr.edu/ ~carter/SAPRC.

Mechanism for 2,3,3,3-Tefralfuoropropene

Alkenes can react in the atmosphere with OH radicals, O_3 or NO_3 radicals, and in general all three need to be taken into account when developing mechanisms for their O_3 formation potential. The rate constants for the reactions of 2,3,3,3-tetrafluoropropene with OH radicals and O_3 have been measured to be 1.05×10^{-12} and 2.77×10^{-21} cm^3 $molec^{-1}$ s^{-1}, respectively (Nielsen et al, 2007). The rate constant for the reaction with O_3 is too low for this reaction to be an important sink compared to reaction with OH radicals, so it can be ignored. The rate constant for reaction with NO_3 radicals have not been measured, but can be estimated by correlation between measured OH and NO_3 radical rate constants for other alkenes (e.g., see Atkinson, 1991; Calvert et al, 2003; Carter, 2000). Based on this correlation, the rate constant for the reactions of 2,3,3,3-tetrafluoropropene is estimated to be less than 10^{-22} cm^3 $molec^{-1}$ s^{-1}, making it negligible under atmospheric conditions. Nielsen et al (2007) obtained a relatively high rate constant of 7.03×10^{-11} cm^3 $molec^{-1}$ s^{-1} for the reactions of this compound with chlorine atoms, but chlorine atom reactions are not expected to be important sinks for VOCs under most atmospheric conditions, including those used for ozone reactivity assessment in this work.

Therefore, the only loss process for 2,3,3,3-tetrafluoropropene that needs to be considered in estimating its ozone impact is reaction with OH radicals. Hurley et al (2007) studied this reaction and found that the major product was $CH_3C(O)F$, with a 91±6% yield. This is consistent with the following mechanism for the OH reaction, and is also consistent with mechanisms for OH reactions with most other alkenes (Calvert et al, 2003; Carter, 2000, 2008):

$$OH + CF_3CF{=}CH_2 \rightarrow CF_3CF(OH)CH_2\cdot$$
$$OH + CF_3CF{=}CH_2 \rightarrow CF_3CF(\cdot)CH_2OH$$
$$CF_3CF(OH)CH_2\cdot + O_2 \rightarrow CF_3CF(OH)CH_2OO\cdot$$
$$CF_3CF(\cdot)CH_2OH + O_2 \rightarrow CF_3CF(OO\cdot)CH_2OH$$
$$CF_3CF(OH)CH_2OO\cdot + NO \rightarrow NO_2 + CF_3CF(OH)CH_2O\cdot$$
$$CF_3CF(OO\cdot)CH_2OH + NO \rightarrow NO_2 + CF_3CF(O\cdot)CH_2OH$$
$$CF_3CF(OH)CH_2O\cdot \rightarrow CF_3C(OH)(\cdot)F + HCHO$$
$$CF_3CF(O\cdot)CH_2OH \rightarrow CF_3C(O)F + \cdot CH_2OH$$
$$CF_3C(OH)(\cdot)F + O_2 \rightarrow HO_2 + CF_3C(O)F$$
$$\cdot CH_2OH + O_2 \rightarrow HO_2 + HCHO$$

or overall:

$$OH + CF_3CF{=}CH_2 \rightarrow CF_3C(O)F + HCHO + HO_2 - NO + NO_2$$

Note that the experimental system of Hurley et al (2007) was such that the predicted formation of formaldehyde as the co-product could not be detected because formaldehyde is formed in the methyl nitrite system they used to generate the OH radicals.

An additional reaction that needs to be considered is the formation of organic nitrates as a minor route in the reaction of peroxy radicals with NO, e.g.,

$$CF_3CF(OH)CH_2OO\cdot + NO \rightarrow CF_3CF(OH)CH_2ONO_2$$

This reaction is assumed to occur ~1.5% of the time in the propene system (Carter, 2009a), but non-carbon substituents are expected to reduce the importance of this reaction further (Carter, 2000, and references therein), so this reaction was neglected in the initial estimates of Carter (2008). However, to fit the chamber data for trans 1,3,3,3-tetrafluoropropene, Carter (2009b) had to assume that nitrate formation in the reaction of the $CF_3CH(OH)CHFOO\cdot$ and $CF_3CH(OO\cdot)CHFOH$ radicals formed in that system occurred ~5% of the time. Since the radicals formed in this case is very similar and isomers of these formed from trans 1,3,3,3-tetrafluoropropene, we initially assume that overall nitrate formation also occurs 5% of the time in the 2,3,3,3-tetrafluoropropene system. However, as discussed below the best fit

to the chamber data were obtained assuming that overall nitrate formation is negligible, so this was used in the final model developed for this project.

The secondary reactions of the products formed also need to be considered when estimating the ozone impacts of a VOC. The reactions of formaldehyde are already incorporated in the base atmospheric chemical mechanism used in this work, which was discussed above (Carter, 2009a). $CF_3C(O)F$ is not expected to react at a significant rate and therefore its subsequent reactions are ignored. It has no known means for it to react with OH radicals or other atmospheric species, and it has no light absorption in the wavelength region important in the lower atmosphere (IUPAC, 2004).

The above discussion focuses on the reactions of the tetrafluoropropene and its oxidation products in the presence of NO_x, which are the major reactions of significance in affecting their ozone impacts. However, to estimate the ultimate environmental fate of this compound and its fluorine-containing products, one needs to also consider the reactions in the absence of NO_x, and the reactions of products formed under such conditions. The most important reactions in the absence of NO_x are reactions of the peroxy radicals with HO_2. For the initially formed peroxy radicals, these include the following:

$$CF_3CF(OH)CH_2OO\cdot + HO_2 \rightarrow O_2 + CF_3CF(OH)CH_2OOH$$
$$CF_3CF(OO\cdot)CH_2OH + HO_2 \rightarrow O_2 + CF_3CF(OOH)CH_2OH$$
$$CF_3CF(OH)CH_2OOH + OH \rightarrow H_2O + CF_3CF(OH)CH_2OO\cdot$$
$$CF_3CF(OO\cdot)CH_2OH + OH \rightarrow H_2O + CF_3CF(OO\cdot)CH_2OH$$
$$CF_3CF(OH)CH_2OOH + h\nu \rightarrow CF_3CF(OH)CH_2O\cdot + OH$$
$$CF_3CF(OO\cdot)CH_2OH + h\nu \rightarrow CF_3CF(O\cdot)CH_2OH + OH$$

The subsequent reactions of the alkoxy radicals formed in the photolyses are as shown above, and the rate constants and photolysis rates are estimated based on those for methyl hydroperoxide. The OH reactions may also occur by abstraction from the C-H bonds in the hydroperoxides but these pathways are estimated to be less important than reaction at the hydroperoxide group and are ignored.

Reactions of the peroxy radicals with other peroxy and acetyl peroxy radicals also need to be considered under low NO_x conditions, though they are less important than the reactions with HO_2 discussed above. These are estimated using the general procedures associated with the SAPRC07 mechanism, as discussed by Carter (2009a) and shown in Table 3 below.

The representation of these reactions in SAPRC-07 mechanism is given in Table 2 and Table 3, which list the model species and reactions, respectively. Table 2 gives a description of the model species used and footnotes to Table 3 indicate the source of the rate constants or parameters used and give additional discussion about how the mechanism was estimated or represented. Carter (2009a) should be consulted for a more complete discussion of the chemical operators and other species used in the SAPRC-07 mechanism. A complete listing of the other reactions used in the SAPRC-07 mechanism for the model simulations for this study is given in Appendix A.

Representation of Chamber Conditions

The procedures used in the model simulations of the environmental chamber experiments for this project are the same as those used by Carter (2009b) for the experiments with trans 1,3,3,3-tetrafluoropropene and are based on those discussed in detail by Carter (2004) and employed in the studies of Carter and Malkina (2005) and Carter et al (2005b), updated for SAPRC-07 as discussed by Carter (2009a). Carter (2004) should be consulted for details of the characterization model and chamber effects parameters employed. The temperatures used when modeling were the averages of the temperatures measured in the reactors, corrected as discussed by Carter (2004).

Table 2. List of model species added to the base mechanism to represent the atmospheric reactions of 2,3,3,3-tetrafluoropropene and its oxidation products

Name	Description
Active Species	
R1234YF	2,3,3,3-tetrafluoropropene
CF3COF	Trifluoroacetyl fluoride
R2F4OOH	$CF_3CF(OOH)CH_2OH$ or $CF_3CF(OH)CH_2OOH$ formed following the reactions of OH with the tetrafluoropropene and reaction of the subsequently formed peroxy radical with HO_2.
RF4OH	$CF_3CF(OH)CH_2OH$ or isomers formed when peroxy radicals formed following OH + tetrafluoropropene reaction reacts by disproportionation with other peroxy radicals.
Steady State Species	
xCF3COF	Formation of trifluoroacetyl fluoride from alkoxy radicals formed in peroxy radical reactions with NO and NO_3 (100% yields) and RO_2 (50% yields)
yRF4OOH	Formation of $CF_3CF(OOH)CH_2OH$ or $CF_3CF(OH)CH_2OOH$ following $RO_2 + HO_2$ reactions.

The light intensity for the blacklight experiments declines slowly with time when the lights are new, though the rate of decline decreases as the lights age (Carter et al, 1995a; Carter, 2004, 2007). The characterization of the light intensity for the previous set of reported experiments is discussed by Carter (2007), and based on extrapolating the light intensity assignments for the experiments carried out then to the current experiments we assign a light intensity corresponding to an NO_2 photolysis rate of 0.115 min^{-1} for the experiments modeled in this report. Model simulations of the control experiments for this and the trans 1,3,3,3-tetrafluoropropene project (Carter, 2009b) indicate that this is an appropriate assignment. The blacklight spectral distribution given by Carter et al (1995a) was found to be appropriate for the blacklights in this chamber and is used when modeling the runs in this chamber using the blacklight light source.

The chamber effects parameters used when modeling the experiments in this chamber were the same as those given by Carter (2004) except for the HONO offgasing parameters, which were derived based on results of characterization runs carried out in conjunction with these experiments as discussed below. As discussed by Carter (2004), the chamber effects model currently used for this chamber represents both the chamber radical source and background NO_x offgasing by HONO offgasing, whose magnitude is determined by the chamber effects parameter RN-I, which is the ratio of the HONO offgasing rate to the NO_2 photolysis rate. The RN-I parameter that best fits the characterization data tends to vary over time depending on the conditions of the chamber, and the results of the characterization experiments applicable to modeling the experiments discussed in this report, and the assignment of the RN-I values used, are given in the Characterization Results section, below.

The initial reactant concentrations used in the model simulations were based on the experimentally measured values. However, the calibration of the 2,3,3,3-tetrafluoropropene measurements were based on calculated amounts of compound injected and the volume of the reactors, which were measured by injecting known quantities of CO or NO_x, and measuring the CO or NO_x using instruments that were independently calibrated.

Table 3. List of reactions and rate constants used to represent the atmospheric reactions of 2,3,3,3-tetrafluoropropene and its oxidation products

Reaction and Products [a]	Rate Parameters [b] k(298)	A	Ea	Refs & Notes [c]
OH + R1234YF = xHO2 + RO2C + xHCHO + xCF3COF + yR2F4OOH	1.05e-12			1
xCF3COF = CF3COF	k is variable parameter: RO2RO			2
xCF3COF = #2 XC	k is variable parameter: RO2XRO			2
yR2F4OOH = R2F4OOH + #-3 XC	k is variable parameter: RO2HO2			2
yR2F4OOH = RF4OH + #-3 XC	k is variable parameter: RO2RO2M			2
yR2F4OOH =	k is variable parameter: RO2RO			2
R2F4OOH + OH = H2O + CF3COF + HCHO + HO2	5.18e-12			3,4
R2F4OOH + HV = OH + CF3COF + HCHO + HO2	Phot Set= COOH			4,5

[a] Format of reaction listing: "=" separates reactants from products; "*#number*" indicates stoichiometric coefficient, "*#coefficient* {*product list*}" means that the stoichiometric coefficient is applied to all the products listed.

[b] Except as indicated, the rate constants are given by $k(T) = A \cdot e^{-Ea/RT}$, where the units of k and A are cm^3 $molec^{-1}$ s^{-1}, Ea are kcal mol^{-1}, T is ^oK, and R=0.0019872 kcal mol^{-1} deg^{-1}. If A and Ea are not given then the rate constant is assumed to be temperature independent. The following special rate constant expressions are used:

Phot Set = *name*: The absorption cross sections and (if applicable) quantum yields for the photolysis reaction are given by Carter (2009a), except for "PAA", which are given below. Here, "*name*" indicates the photolysis set used. Photolysis rates used in chamber and ambient simulations are given in Table A-3.

k is variable parameter *name*: The rate constant is calculated using variable parameters that are calculated using concentrations of various species. See Footnotes [c] and [e] to Table A-2 in Appendix A for a discussion of the parameters and how they are calculated.

[c] Footnotes discussing reactions or rate constants used are as follows:

1 See text for a discussion of the mechanism. The rate constant is from Nielsen et al (2007). Overall organic nitrate formation is assumed to be negligible because this was found to give the best fits to the chamber data, as discussed in the Results section.

2 See Carter (2009a) and footnotes to Table A-2 for a discussion of the reactions of peroxy radical operator species. xCF3COF is the operator that represents the formation of trifluoroacetyl fluoride from peroxy radical reactions. YR2F4OOH is the operator that represents the formation of tetrafluorohyderoperoxides formed when the peroxy radicals from the OH + tetrafluoropropene reactions react with HO_2.

3 The reaction is assumed to occur primarily with OH abstracting from the OOH group, with a rate constant assumed to be the same as used for that process in the reaction of OH with methylhydroperoxide (COOH). See Table A-2.

4 The alkoxy radicals formed should be the same as those formed in the OH + tetrafluoropropene reaction, so the same overall products are assumed to be formed, i.e., HO2 + HCHO + trifluoroacetyl fluoride.

5 The photolysis is assumed to occur at the same rate as used for methyl hydroperoxide, and the products are assumed to be OH + the alkoxy radical. See Carter (2009a).

Atmospheric Reactivity Simulations

Atmospheric reactivity model simulations were carried out to derive MIR and other atmospheric reactivity values for 2,3,3,3-tetrafluoropropene. The base mechanism, scenarios, and methods used were the same as those used when calculating the MIR and other atmospheric ozone reactivity scales for the SAPRC-07 mechanism by Carter (2009a), so the atmospheric reactivities calculated for 2,3,3,3-tetrafluoropropene reactivities in this work are directly comparable with those given by Carter (2009a) for the ~1100 other types of VOCs represented using the SAPRC-07 mechanism. The mechanism used for 2,3,3,3-tetrafluoropropene is the same as gave the best fits to the results of the chamber simulations, as discussed in the Results section below, and is given in Table 3, above. The inputs used in the reactivity scenarios are described by Carter (1994a,b).

RESULTS AND DISCUSSION

A chronological listing of the environmental chamber experiments carried out for this project is given in Table 4. These include experiments with 2,3,3,3-tetrafluoropropene and appropriate characterization and control experiments needed for the data to be useful for mechanism evaluation. The results of the characterization experiments will be discussed first, followed by a discussion of the results of the mechanism evaluation experiments and of the model simulations of these experiments.

Characterization Results

The individual characterization experiments that are relevant to this project are summarized in Table 4. Except as discussed below, the characterization results are consistent with those discussed by Carter et al (2005b), Carter and Malkina (2005, 2007), Carter (2007) and Carter (2009b), and the same characterization parameters were used for modeling. The only chamber effect parameter that was changed when modeling the experiments for this project concerns the apparent HONO offgasing, which is believed to be responsible for both the chamber radical source and NO_x offgasing effects (Carter, 2004). This is represented in the chamber effects model by the parameter RN-I, which is the HONO offgasing rate used in the simulations divided by the light intensity as measured by the NO_2 photolysis rate. Figure 3 shows the HONO offgasing parameters that best fit the radical or NO_x - sensitive characterization experiments carried out in the UCR EPA during the period of the last three sets of reactors. Note that the best-fit parameters depend on the mechanism used (particularly the OH + NO_2 rate constant), and all these were calculated for SAPRC-07, the mechanism used in this work.

The experiments carried out for this project start at run EPA966, so the applicable characterization data is for the last set of reactors shown on the figure. The average RN-I parameter that fit the results of the experiments with this reactor was approximately 10 ppt, and this was used when modeling the experiments carried out for this project. Although there is a large amount of scatter in the RN-I parameter that gave the best fit to the data in these characterization experiments, it should be noted that the simulation of the surrogate - NO_x incremental reactivity experiments, which are the experiments used for mechanism evaluation, are not very sensitive to this parameter. Test calculations showed that variation of this parameter within the range shown on Figure 4 has only a minor effect on the simulations of these experiments, and does not affect conclusions concerning the tetrafluoropropene mechanism that gives the best fits to the data.

For modeling purposes, we use the same chamber effects parameters as used by Carter (2004), Carter and Malkina (2005), Carter et al (2005b), and Carter (2007) for all the other chamber effect parameters. Simulations of the incremental reactivity experiments are also not very sensitive to these parameters.

Other control experiments carried out during this period were two side equivalency tests (with the same reactive organic gas surrogate - NO_x mixture simultaneously irradiated in both reactors). In addition, a propene - NO_x control experiment and several pure air runs were carried out previously, and the results were as expected. The results of the side equivalency tests indicated acceptable side equivalency and are given in Table 5, in conjunction with the results of the reactivity experiments with 2,3,3,3-tetrafluoropropene, discussed below.

Table 4. Summary of experiments carried out for this project.

Run [a]	Date	Type [b]	Purpose and Applicable Conditions	Results
966	1/8/09	Surrogate - NO_x Irradiation	Control for incremental reactivity experiments to test side equivalency. See Table 5 for reactant levels.	Initial concentrations in the appropriate range. Relevant results are summarized on Table 5. Good side equivalency obtained.
971	1/19/09	CO - NO_x Irradiation	Chamber radical source characterization. 22 ppb NO_x and 38 ppm CO injected into both reactors	Results indicated much lower radical input rates than generally observed in such experiments, but was not completely outside the range of variability observed previously. See Figure 3.
976	2/21/09	Surrogate - NO_x + 2,3,3,3-tetrafluoropro-pene Irradiation	Incremental reactivity experiment for 2,3,3,3-tetrafluoropropene. See Table 5 for reactant levels.	Initial concentrations not in the appropriate range; NO_x levels lower than expected and gas ROG surrogate levels high because of an injection calculation error. No PM data. See Table 5 and Figure 4.
981	3/19/09	Surrogate - NO_x + 2,3,3,3-tetrafluoropro-pene Irradiation	Incremental reactivity experiment for 2,3,3,3-tetrafluoropropene. See Table 5 for reactant levels.	Run ended early because of probable leak in reactor. Initial concentrations not in the appropriate range; NO_x levels higher than expected and gas ROG surrogate levels high because of an injection calculation error. PM data are questionable and are not used. See Table 5 and Figure 4.
982	3/20/09	CO - Air Irradiation	Chamber NO_x offgasing characterization. 36 ppm CO injected into both reactors.	Results were consistent with chamber wall model used for these experiments. See Figure 3.
984	3/26/09	Surrogate - NO_x + 2,3,3,3-tetrafluoropro-pene Irradiation	Incremental reactivity experiment for 2,3,3,3-tetrafluoropropene. See Table 5 for reactant levels.	Initial concentrations not in the appropriate range; gas ROG surrogate levels high because of an injection calculation error. See Table 5 and Figure 4.
985	3/30/09	Surrogate - NO_x + 2,3,3,3-tetrafluoropro-pene Irradiation	Incremental reactivity experiment for 2,3,3,3-tetrafluoropropene. See Table 5 for reactant levels	Initial concentrations not in the appropriate range; gas ROG surrogate levels high because of an injection calculation error. See Table 5 and Figure 4.

Table 4 (continued)

Run [a]	Date	Type [b]	Purpose and Applicable Conditions	Results
986	4/1/09	Surrogate - NO_x + 2,3,3,3-tetrafluoropro-pene Irradiation	Incremental reactivity experiment for 2,3,3,3-tetrafluoropropene. See Table 5 for reactant levels	Initial concentrations not in the appropriate range; gas ROG surrogate levels high because of an injection calculation error. See Table 5 and Figure 4.
990	4/8/09	Surrogate - NO_x + 2,3,3,3-tetrafluoropro-pene Irradiation	Incremental reactivity experiment for 2,3,3,3-tetrafluoropropene. See Table 5 for reactant levels. Base case is standard MIR conditions	Initial concentrations in the appropriate range. See Table 5 and Figure 4. No useable PM data.
991	4/9/09	Surrogate - NO_x + per-fluorohexane Irradiation	Control for incremental reactivity experiments to test side equivalency and to verify that the addition of the perfluoro n-hexane dilution tracer does not affect reactivity results. Standard MIR conditions except that 3.5 ppm pefluorohexane added to Side A. See Table 5 for other reactant levels..	Initial concentrations in the appropriate range. Relevant results are summarized on Table 5. Good side equivalency obtained. As expected, the presence of perfluorohexane did not affect the gas-phase results. No useable PM data.
992	4/10/09	Surrogate - NO_x + 2,3,3,3-tetrafluoropro-pene Irradiation	Incremental reactivity experiment for 2,3,3,3-tetrafluoropropene. See Table 5 for reactant levels. Base case is standard MIR conditions	Injected NO_x levels lower than intended due to injection error . See Table 5 and Figure 4.
1000	4/23/09	CO - air irradiation and halopropene light decay test.	~65 ppm of CO and ~ 1 ppm each of 2,3,3,3-tetrafluoropropene, trans 1,3,3,3-tetrafluoropropene, another halogenated propene, perfluorohexane and n-butane were injected into both reactors and irradiated. [a]	The ozone formation in this experiment was consistent with that expected using the standard chamber characterization model. See Figure 3. The fluoropropene results indicated that concentrations of 2,3,3,3-tetrafluoropropene decline at the same rates as CO and n-butane, which is attributable to dilution. However, the added trans 1,3,3,3-tetrafluoropropene and another halopropene declined in the reactor slightly faster than can be accounted for gas-phase processes.
1004	5/3/09	CO - NO_x Irradiation	40 ppb of CO and 20 ppb of NOx and ~50 ppb perfluorohexane injected into both reactors.	The NO oxidation rate in this experiment was in the range expected using the standard chamber characterization model. See Figure 3.

Table 4 (continued)

Run [a]	Date	Type [b]	Purpose and Applicable Conditions	Results
1005	5/4/09	Surrogate - NO_x + 2,3,3,3-tetrafluoropro-pene Irradiation	Incremental reactivity experiment for 2,3,3,3-tetrafluoropropene. See Table 5 for reactant levels. Base case is standard MIR conditions.	Run had to be ended just after 5 hours because of leakage in base case reactor. Initial concentrations in the appropriate range. M-Xylene data for test experiment, and therefore IntOH reactivity data, questionable and inconsistent with data from other GC instruments. See Table 5 and Figure 4.

[a] Gaps in run number indicate experiments whose data were not useful for this project..

[b] All experiments are ~6-hour irradiations using blacklights. "Surrogate" indicates a ROG surrogate - NO_x mixture irradiated; "MIR" and "MOIR/2" mean the target initial NO_x and base ROG surrogate were 30 ppb and 0.55 ppmC and 25 ppb and 1.1 ppmC, respectively. "Incremental Reactivity" indicates that a reactant was added to one of the two reactors.

[c] The purpose of injecting the n-butane and halopropenes was to test whether consumption of halopropenes occur at faster rates in this reactor than can be accounted for by gas-phase processes. Loss of these compounds by reaction with OH radicals is calculated to be negligible under the conditions of these experiments. The n-butane was injected as a control and dilution tracer because it is known not to have unknown loss processes and can be analyzed with precision. The perfluorohexane data were not useful as a tracer because of GC interferences.

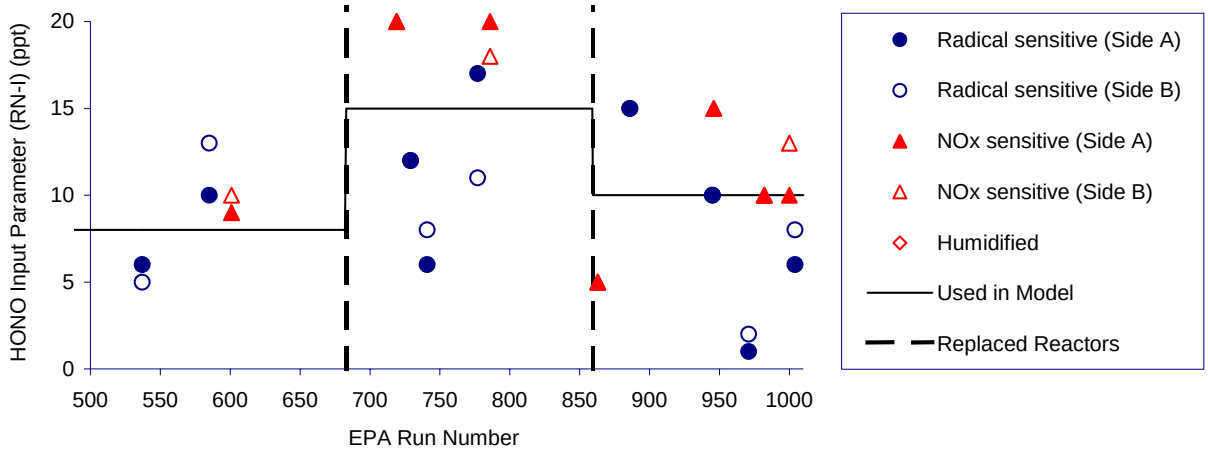

Figure 3. Plots of best fit HONO offgasing parameters against UCR EPA run number.

Incremental Reactivity and Mechanism Evaluation Results

The conditions and selected results of the incremental reactivity experiments used to evaluate the 2,3,3,3-tetrafluoropropene mechanism are summarized on Table 5. These experiments consist of irradiations of a reactive organic gas (ROG) - NO_x mixture serving as a simplified model of the chemical system involved on O_3 formation in urban atmospheres, together in irradiations of the same mixture with 2,3,3,3-tetrafluoropropene (the test compound) added. The experiment without the added test compound is referred to as the "base case" experiment, and the experiment where the test compound is added is the "test" experiment. The differences in O_3 formation and other measures of reactivity in these experiments provide a measure of the effects of the test compound in a system more closely representing atmospheric conditions than the simpler experiments discussed above, and provide a more realistic test of the mechanism's ability to predict its atmospheric reactivity.

As in previous incremental reactivity experiments carried out in this chamber (Carter and Malkina, 2005, 2007; Carter et al, 2005b), the plan for this project was to carry out two types of base case experiments. The first is a lower ROG/NO_x experiment designed to approximate conditions where O_3 formation is most sensitive to VOC emissions, which serve as the basis for the MIR reactivity scale, and are referred to as "MIR" experiments. The second is at higher ROG/NO_x ratios with NO_x levels at approximately half that yielding maximum ozone concentrations, and are referred to as "MOIR/2" experiments. For the MIR experiments the target initial NO_x was approximately 30 ppb and the target initial base case ROG was approximately 0.6 ppmC, while for the MOIR/2 experiments the target initial levels were approximately 25 ppb and 2.3 ppmC, respectively. In both cases, the base ROG surrogate mixture representing reactive organic gases from all sources consists of n-butane, n-octane, ethene, propene, trans-2-butene, toluene and m-xylene, and is based on a mixture derived previously (Carter et al, 1995b) as a simplification of ambient mixtures used in the atmospheric reactivity calculations. Earlier versions of this mixture also contained formaldehyde, but this was not included in the current experiments for experimental reasons. As discussed by Carter and Malkina (2005), this does not significantly affect the utility of the experiments for mechanism evaluation.

Although the plan for the project was to carry out several MIR and MOIR/2 experiments, problems were encountered in the calculations of injections or the injection procedures for many of the experiments, resulting in initial concentrations being different than those intended. These cases are noted where applicable in Table 4 and Table 5. Since the injection errors were applicable for both the base case and the added test compound side, these experiments were still valid as incremental reactivity experiments. Although these experiments did not have the desired initial base case ROG and/or NO_x levels, they were still useful for mechanism evaluation because the variability in initial reactant concentrations are taken into account in the model calculations The net effect of including these experiments is that the mechanism is evaluated under a wider range of conditions than would otherwise be the case. The experiments modeled include one MIR experiment and a number of experiments with lower ROG/NO_x levels, so the conditions intended to be used in the project plan are included.

The measures of gas-phase reactivity used to evaluate the mechanisms in the incremental reactivity experiments are the effects of the test compound on $\Delta([O_3]-[NO])$, or $([O_3]_t-[NO]_t)-([O_3]_0-[NO]_0)$, and IntOH, the integrated OH radical levels. As discussed elsewhere (e.g., Johnson, 1983; Carter and Atkinson, 1987; Carter and Lurmann, 1991, Carter et al, 1993), $\Delta([O_3]-[NO])$ gives a direct measure of the amount of conversion of NO to NO_2 by peroxy radicals formed in the photooxidation reactions, which is the process that is directly responsible for ozone formation in the atmosphere. This gives a useful measure of factors affecting O_3 reactivity even early in the experiments where O_3 formation is suppressed by the unreacted NO. Although this is the primary measure of the effect of the VOC on O_3 formation, the

Table 5. Summary of initial concentrations and selected gas-phase results of the incremental reactivity experiments.

EPA Run No.	Test Side	Test Cmpd Added (ppm)	Base Run Initial Concentrations		5 Hr O_3 (ppb)		D([O_3]-[NO]) Change (ppb)		IntOH change (ppt-min)	5 Hr PM ($\mu g/m^3$)	
			NO_x (ppb)	ROG (ppmC)	Base	Test	2 Hr	5 Hr		Base	Test
Side Equivalency or added Perfluorohexane Experiments											
966	A		22	1.23	89	89	3	0	0	0.36	0.31
991	A	3.49 [a]	33	0.54	37	37	1	0	1	[b]	[b]
Added 2,3,3,3-Tetrafluoropropene Experiments (in order of increasing base case ROG/NO_x)											
1005	A	2.12	32	0.54	29	111	33	-46	18	[b]	[b]
990	B	1.82	33	0.64	52	125	37	73	[b]	[b]	[b]
986	B	2.18	34	1.44 [c]	117	152	34	34	-4	0.01	0.01
985	B	1.12	25	1.54 [c]	107	122	10	15	-3	0.05	0.04
981	B	1.26	41	2.61 [c]	[b]	[b]	14	[b]	[b]	[b]	[b]
992	A	2.37	15 [d]	1.06	72	101	22	29	-7	0.23	0.02
976	A	1.05	13 [d]	1.31 [c]	82	95	8	10	-2	0.11	0.04
984	B	1.11	23	3.13 [c]	91	98	3	7	0	0.26	0.26

[a] Run carried out with added prefluorohexane to verify that this compound is unreactive and its presence would not affect reactivity results.

[b] No useable data obtained or experiment ended before 5 hours.

[c] Gaseous base ROG components (ethene, propene, and trans-2-butene) high by a factor of 3.6 due to reactant injection calculation error.

[c] Initial NO_x levels lower than intended due to NO_x injection problems.

effect on radical levels is also a useful measure for mechanism evaluation, because radical levels affect how rapidly all VOCs present, including the base ROG components, react to form ozone.

The integrated OH radical levels are not measured directly, but can be derived from the amounts of consumption of reactive VOCs that react only with OH radical levels. In particular,

$$\mathrm{IntOH}_t = \frac{\ln([\mathrm{tracer}]_0 / [\mathrm{tracer}]_t) - Dt}{k\mathrm{OH}^{\mathrm{tracer}}} \qquad \text{(I)}$$

where $[\mathrm{tracer}]_0$ and $[\mathrm{tracer}]_t$ are the initial and time t concentrations of the compound used as the OH tracer, $k\mathrm{OH}^{\mathrm{tracer}}$ its OH rate constant, and D is the dilution rate in the experiments. The latter is neglected in our IntOH analysis. The base ROG surrogate component m-xylene was used as the tracer to derive the IntOH levels in these experiments. The OH + m-xylene rate constant used was 2.36×10^{-11} cm^3 $molec^{-1}$ s^{-1} (Atkinson, 1989).

Plots of experimental $\Delta([O_3]-[NO])$ in the base case and test experiments, changes in $\Delta([O3]-[NO])$ and IntOH caused by adding the 2,3,3,3-tetrafluoropropene, are shown on Figure 4 and changes in these quantities are also summarized on Table 5. It can be seen that the addition of the tetrafluoropropene caused a measurable increase in NO oxidation and O_3 formation in all the experiments, though the increase was small in some of the experiments with high ROG/NO_x ratios and lower amount of test compound added. The effect of adding a given amount of the tetrafluoropropene on $\Delta([O_3]-[NO])$

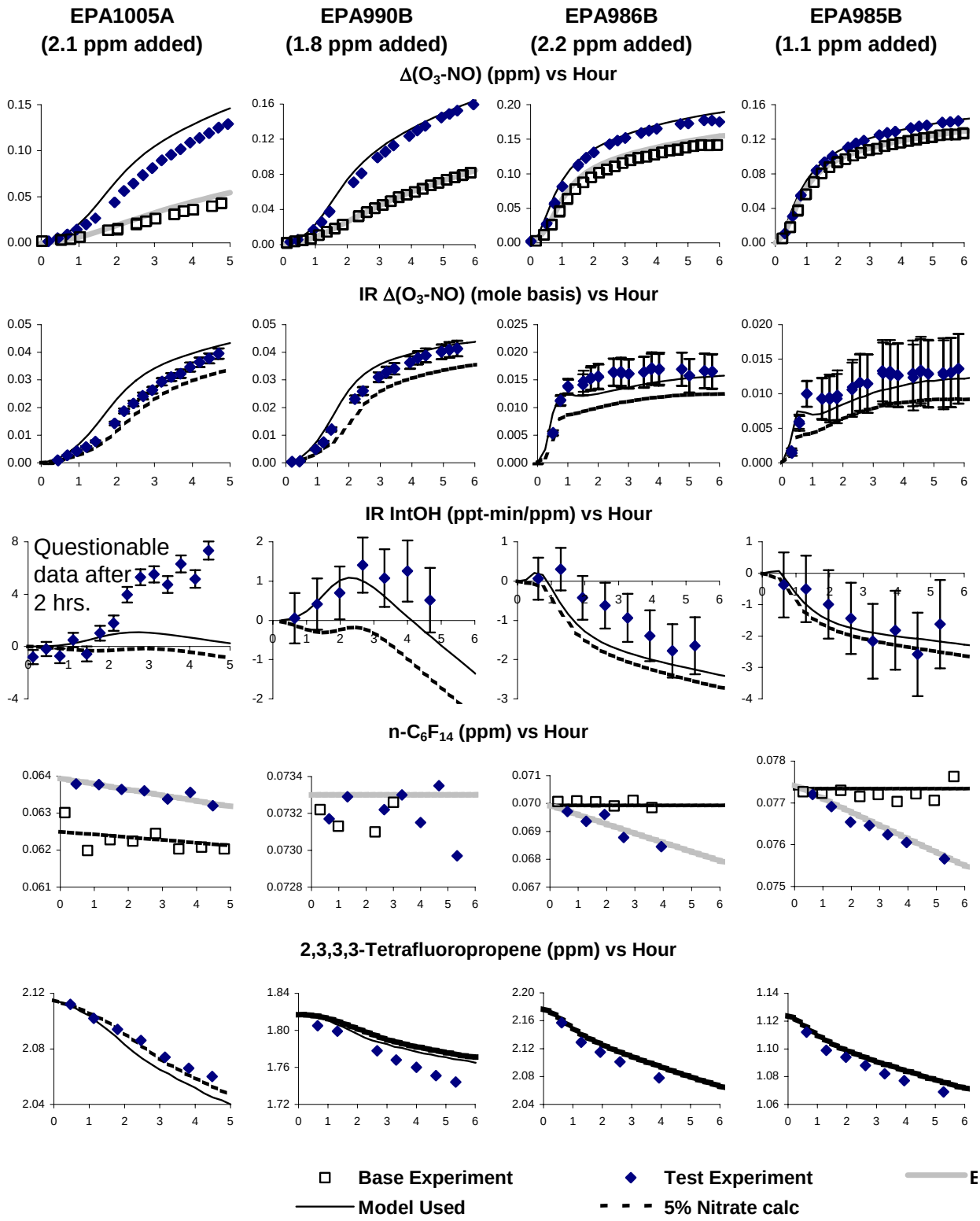

Figure 4a. Experimental and calculated results of the incremental reactivity experiments with added 2,3,3,3-tetrafluoropropene (part 1 of 2).

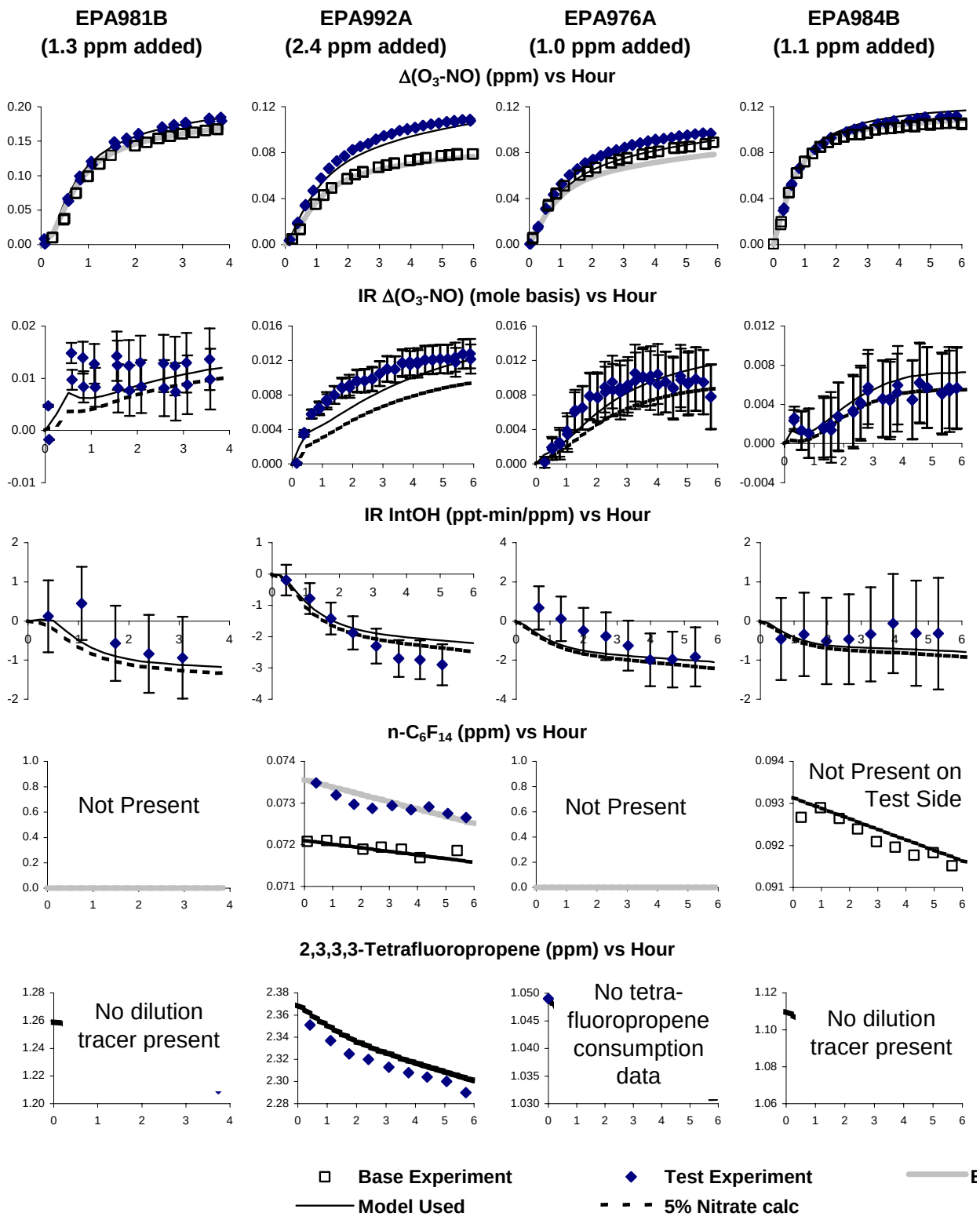

Figure 4b Experimental and calculated results of the incremental reactivity experiments with added 2,3,3,3-tetrafluoropropene (part 2 of 2).

was larger in the MIR experiment than the lower NO_x runs, which is expected since MIR conditions are generally more sensitive to most VOCs.

The effects of the added tetrafluoropropene on the integrated OH levels in the experiments were relatively low, though generally negative. This indicates that this compound has a tendency to inhibit radical levels in the experiments, though the effect is small. Many VOCs have a tendency to inhibit overall radical levels in experiments to varying degrees.

Results of model simulations of the incremental reactivity experiments are also shown on Figure 4. For most experiments the model simulated the Δ([O3]-[NO]) results of the base case experiment quite well. The best fits to the Δ([O_3]-[NO]) incremental reactivity data were obtained if it is assumed that no nitrate formation occurs in the overall reaction, as shown with the solid line ("model used") curves on Figure 4. It is assumed that overall nitrate formation occurs with a ~5% yield, which gives best fits to the data for trans 1,3,3,3-tetrafluoropropene (Carter, 2009b), then the model has a small but consistent bias towards underpredicting Δ([O_3]-[NO]) reactivities, as shown by the dashed lines on Figure 4. Changing the overall nitrate yield has no significant effect on calculations of IntOH reactivity or the rates of tetrafluoropropene consumption.

Figure 4 also shows the experimental and model calculated data for the consumption of the 2,3,3,3-tetrafluoropropene during the experiment. In all cases the consumption of this compound was relatively slow and the fractions reacted were low. Because even relatively low levels of reactor dilution would affect consumption data for such slowly reacting compounds, in most experiments we added perfluoro n-hexane as a tracer to determine dilution rates to use when modeling these experiments. The results indicated that some dilution was occurring in some experiments but not in others, though the dilution rates were never greater than 0.5% per hour. Although small, this level of dilution did have an effect on the model simulations of the tetrafluoropropene consumption rate, so dilution rates adjusted to fit the perfluorohexane data were used when modeling runs where perfluorohexane data were available.

Figure 4 shows that even after correcting for dilution the model still had a slight tendency to underpredict the consumption rates of 2,3,3,3-tetrafluoropropene to a slight extent for most of the experiments. However, this underprediction was also seen for n-butane, which is present in all experiments as a base ROG surrogate, and which also reacts relatively slowly (though with a rate constant that is about 2.3 times higher than the tetrafluoropropene. The consumption rate of the tetrafluoropropene relative to n-butane, after correction for dilution in most cases, agreed very well with the rate constant ratios for these two compounds, indicating that this underprediction is not a problem with the rate constants used in the mechanisms. It is apparently due to the model somewhat underpredicting OH levels in the experiments. Since the model gives reasonably good fits to the IntOH reactivity, this underprediction must be occurring to the same extent in the base case experiments, and indicates a problem with the base mechanism, not the mechanism for the 2,3,3,3-tetrafluoropropene.

Measurements of particle formation were also made during the course of the experiments, using the procedures discussed above and by Carter et al (2005b), and representative results are summarized on Table 5. The addition of the 2,3,3,3-tetrafluoropropene was found to have either no measurable effect on PM formed or to decrease PM formed in the experiments, indicating that this compound is not a significant source of secondary organic aerosol (SOA). This is not unexpected, since the mechanism derived for this compound does not involve formation of low volatility products. Slight inhibiting effects on SOA is similar to what Carter et al (2005a) observed for ethylene and propylene glycols, and is attributed to the slightly negative effects of these compounds on overall radical levels, which causes less SOA formation from the base ROG surrogate components.

Atmospheric Reactivity Calculation

Conditions and maximum O_3 concentrations of the ambient scenarios used for reactivity assessment are summarized on Table 6. These are the same scenarios as used to calculate the atmospheric reactivities of the ~1100 types of VOCs using the SAPRC-07 mechanism by Carter (2009a), and are also the same as used in previous reactivity scales calculated using the SAPRC-99 (Carter, 2000a), and SAPRC-90 (Carter, 1994a) mechanisms. All of these are 1-day box model scenarios with varying inversion heights, initially present and emitted NO_x and reactive organics, and O_3 and background VOCs entrained from aloft as the inversion heights increase during the day (Carter, 1994a,b), with inputs designed to represent various urban areas around the United States (Baugues, 1990). As discussed previously, four types of scenarios are employed.

- Base. The base case scenarios have the NO_x and other inputs as originally specified by Baugues (1990) to represent the various urban areas around the United States. Note that these are not good representations of current conditions, since generally these scenarios predict much higher O_3 levels than currently occur, and these box model incorporate significant simplifications of transport, mixing, and emissions, and multi-day effects, which can be important. However, they do represent a variety of chemical conditions, which are the main factors reflecting *relative* atmospheric reactivities of VOCs. These scenarios represent a variety of relative NO_x levels, which is a major factor affecting absolute and relative reactivities of VOCs (Carter and Atkinson, 1989; Carter, 1994a). For this reason, other types of scenarios, discussed below, are derived to represent standard conditions of NO_x availability.

- MIR. The Maximum Incremental Reactivity (MIR) scenarios have the NO_x inputs adjusted so that the base ROG mixture used to represent all the anthropogenic VOC emissions has the maximum incremental reactivity relative to ozone formation. All the other inputs are the same as in the base case scenarios. Although the base ROG reactivity is used to define the MIR NO_x level, most other types of VOCs also have their maximum incremental reactivity at this same NO_x level. These scenarios represent the relatively high NO_x conditions where O_3 formation is the most sensitive to VOC emissions. The averages incremental reactivities in all these scenarios are used to derive the MIR scale that is used in regulatory applications in California (CARB 1993, 2000).

- MOIR. The Maximum Ozone Incremental Reactivity (MOIR) scenarios have the NO_x inputs adjusted to give the maximum daily maximum ozone concentration. All other inputs are the same as in the base and MIR scenarios. These scenarios represent NO_x conditions that are optimum for O_3 formation, which is always lower than those for MIR. The averages incremental reactivities in all these scenarios are used to derive the MOIR scale, which can be considered as an alternative to MIR (Carter, 1994a).

- EBIR. The Equal Benefit Incremental Reactivity (EBIR) scenarios have the NO_x inputs adjusted so that O_3 formation is equally sensitive to changes in total ROG or NO_x inputs. All the other inputs are the same as in the base, MIR, and MOIR scenarios. The NO_x inputs are always lower than those yielding maximum O_3 (MOIR), and represent the lowest NO_x levels where VOC control is at least as effective as NO_x control. The averages incremental reactivities in all these scenarios are used to derive the EBIR scale, which is a useful complement to the MIR scale in assessing how NO_x levels affect relative reactivities.

- Averaged Conditions. The averaged conditions scenarios have all inputs other than total NO_x derived to represent the average for the base case scenarios. The NO_x inputs are varied to assess how measures of reactivity depend on NO_x with other inputs held constant. Incremental reactivities in the MIR, MOIR, and EBIR averaged conditions scenarios (i.e., whose NO_x inputs are adjusted to represent those respective conditions) usually give good approximations to reactivities in those respective scales, though they are not used in deriving these scales.

Table 6. Summary of conditions of scenarios used for reactivity assessment

Scenario	Max O_3 (ppb)				ROG / NOx				Max Height (kM)	ROG input (m.mol m^{-2})	O_3 aloft (ppb)	Final H (m)
	Base	MIR	MOIR	EBIR	Base	MIR	MOIR	EBIR				
Averaged Conditions		178	225	211		3.9	5.9	9.1	1.8	15	70	1823
Atlanta, GA	171	144	176	168	7.3	3.7	5.6	7.9	2.1	12	63	2146
Austin, TX	170	153	185	175	9.3	3.5	5.4	8.2	2.1	11	85	2108
Baltimore, MD	310	243	318	293	5.2	4.0	6.2	10.1	1.2	17	84	1169
Baton Rouge, LA	234	185	234	224	6.8	4.5	6.6	8.7	1.0	11	62	968
Birmingham, AL	238	203	257	242	6.9	2.8	4.3	6.4	1.8	13	81	1770
Boston, MA	191	164	199	189	6.5	2.9	4.4	6.8	2.6	14	105	2598
Charlotte, NC	139	137	162	158	7.8	1.9	3.0	4.1	3.0	7	92	3046
Chicago, IL	284	241	320	299	11.6	4.4	6.6	9.9	1.4	25	40	1392
Cincinnati, OH	195	158	197	182	6.4	3.5	5.3	9.1	2.8	17	70	2816
Cleveland, OH	241	194	241	228	6.6	4.4	6.9	10.3	1.7	16	89	1650
Dallas, TX	184	160	202	192	4.7	4.2	6.4	9.2	2.3	18	75	2250
Denver, CO	193	161	199	187	6.3	5.0	7.6	11.6	3.4	29	57	3358
Detroit, MI	235	183	238	218	6.8	3.8	5.8	10.0	1.8	17	68	1844
El Paso, TX	175	144	175	168	6.6	4.6	7.2	10.0	2.0	12	65	2000
Hartford, CT	167	145	184	173	8.4	2.9	4.5	7.3	2.3	11	78	2318
Houston, TX	298	226	298	277	6.1	4.1	6.2	9.5	1.7	25	65	1748
Indianapolis, IN	202	156	203	191	6.6	4.0	6.5	9.8	1.7	12	52	1675
Jacksonville, FL	149	126	156	149	7.6	3.7	5.5	7.6	1.5	8	40	1485
Kansas City, MO	151	126	158	146	7.1	3.1	4.9	8.5	2.2	9	65	2200
Lake Charles, LA	288	229	305	291	7.4	3.6	5.3	7.2	0.5	7	40	457
Los Angeles, CA	558	403	559	528	7.6	5.2	8.0	11.2	0.5	23	100	503
Louisville, KY	201	162	202	192	5.5	3.3	5.1	7.4	2.5	14	75	2518
Memphis, TN	223	178	231	216	6.8	3.4	5.1	7.8	1.8	15	58	1750
Miami, FL	129	120	149	143	9.6	2.9	4.5	6.4	2.7	9	57	2720
Nashville, TN	161	146	186	175	8.0	2.6	4.0	6.0	1.6	7	50	1608
New York, NY	372	302	378	357	8.1	4.8	6.7	9.8	1.5	39	103	1512
Philadelphia, PA	234	178	234	218	6.2	4.1	6.3	9.7	1.8	19	53	1800
Phoenix, AZ	267	208	267	244	7.6	5.0	7.8	13.0	3.3	40	60	3250
Portland, OR	159	131	163	156	6.5	3.1	4.9	7.0	1.6	6	66	1575
Richmond, VA	231	181	233	214	6.2	3.6	5.5	9.4	1.9	16	64	1932
Sacramento, CA	195	150	196	183	6.6	3.9	6.0	9.1	1.1	7	60	1103
St Louis, MO	304	237	311	288	6.1	4.7	7.2	11.6	1.6	26	82	1625
Salt Lake City, UT	180	156	189	177	8.5	3.5	5.5	9.1	2.2	11	85	2150
San Antonio, TX	119	101	122	118	3.9	3.0	4.7	6.5	2.3	6	60	2308
San Diego, CA	185	146	185	177	7.1	4.7	7.2	10.1	0.9	8	90	850
San Francisco, CA	225	345	455	434	4.8	6.1	9.0	12.0	0.7	25	70	650
Tampa, FL	212	172	218	209	4.4	3.5	5.2	7.0	1.0	8	68	991
Tulsa, OK	219	171	219	202	5.3	3.5	5.4	8.8	1.8	15	70	1830
Washington, DC	272	209	273	256	5.3	3.2	4.8	7.4	1.4	13	99	1421

Table 7 gives the calculated incremental reactivities for 2,3,3,3-tetrafluoropropene in these various scenarios. These were calculated using the mechanism that gave the best fit to the chamber data, i.e. with the nitrate yield set at 5% (see Table 3). The calculated incremental reactivities for ethane, the compound that has been used by the U.S. EPA as the informal standard to define "negligible" ozone impact for the purpose of exempting VOCs from regulation as ozone precursors (Dimitriades, 1999), are also shown on the table. Plots of the incremental reactivities of 2,3,3,3-tetrafluoropropene relative to ethane against relative NO_x levels are shown on Figure 5

It can be seen that although its incremental reactivities of 2,3,3,3-tetrafluoropropene are always positive, they are relatively low, and are comparable, on a mass basis, to those for ethane. The reactivity relative to ethane shows relatively little variability from scenario to scenario, with the mass-based reactivity ratio for all scenarios being 0.9±0.2. The reactivity ratio for the MIR scenarios is slightly higher being 1.04±0.13, but the reactivities of these two compounds are still well within the variability from scenario to scenario.

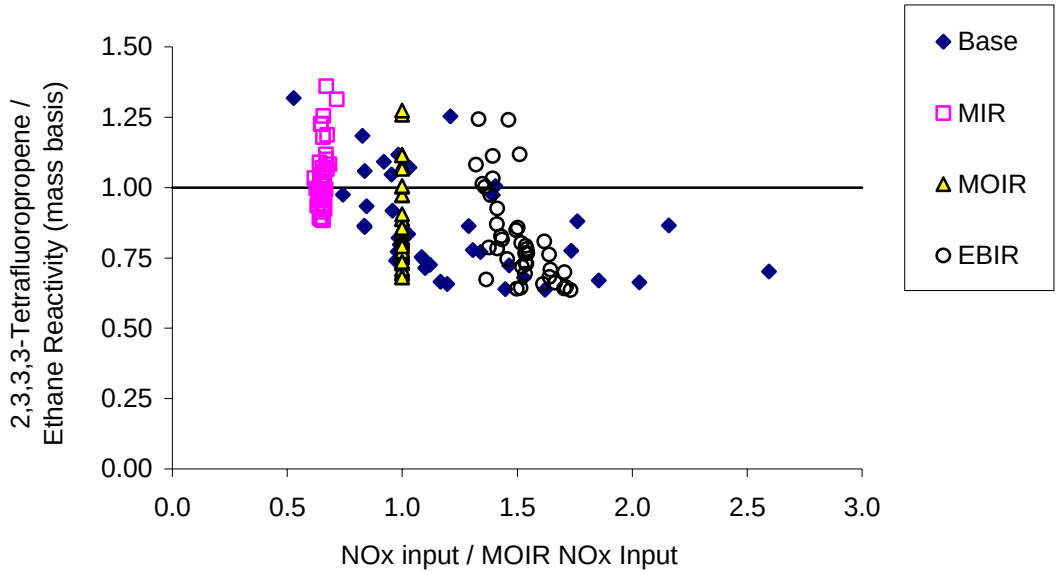

Figure 5. Plots of reactivities of 2,3,3,3-tetrafluoropropene relative to ethane against relative NO_x levels for all the scenarios used for reactivity assessment.

Table 7. Calculated atmospheric incremental reactivities for 2,3,3,3-tetrafluoropropene and ethane.

Scenario	2,3,3,3-Tetrafluoropropene Incremental Reactivity (gm O_3 / gm VOC)				Ethane Incremental Reactivity (gm O_3 / gm VOC)			
	Base	MIR	MOIR	EBIR	Base	MIR	MOIR	EBIR
Averaged Conditions		0.273	0.152	0.103		0.268	0.184	0.130
Reactivity Scale Value (Scenario averages)	0.135 ±0.035	0.267 ±0.047	0.151 ±0.025	0.104 ±0.018	0.162 ±0.043	0.264 ±0.065	0.184 ±0.051	0.133 ±0.038
Atlanta, GA	0.121	0.266	0.159	0.112	0.140	0.252	0.179	0.129
Austin, TX	0.103	0.268	0.162	0.112	0.132	0.276	0.208	0.146
Baltimore, MD	0.179	0.256	0.136	0.091	0.208	0.254	0.178	0.128
Baton Rouge, LA	0.131	0.232	0.139	0.097	0.123	0.196	0.129	0.090
Birmingham, AL	0.110	0.325	0.171	0.117	0.173	0.351	0.245	0.183
Boston, MA	0.112	0.259	0.152	0.109	0.155	0.276	0.201	0.149
Charlotte, NC	0.087	0.272	0.172	0.134	0.124	0.306	0.242	0.199
Chicago, IL	0.078	0.255	0.133	0.089	0.089	0.239	0.149	0.104
Cincinnati, OH	0.135	0.279	0.159	0.106	0.206	0.306	0.229	0.165
Cleveland, OH	0.150	0.236	0.143	0.097	0.164	0.217	0.158	0.115
Dallas, TX	0.230	0.237	0.139	0.094	0.236	0.232	0.165	0.116
Denver, CO	0.184	0.231	0.138	0.096	0.156	0.184	0.123	0.086
Detroit, MI	0.125	0.268	0.144	0.095	0.188	0.288	0.206	0.148
El Paso, TX	0.158	0.229	0.140	0.097	0.145	0.186	0.132	0.094
Hartford, CT	0.111	0.302	0.176	0.120	0.166	0.322	0.247	0.183
Houston, TX	0.145	0.269	0.141	0.093	0.188	0.277	0.185	0.128
Indianapolis, IN	0.159	0.289	0.163	0.111	0.191	0.280	0.194	0.138
Jacksonville, FL	0.119	0.297	0.169	0.120	0.122	0.270	0.174	0.123
Kansas City, MO	0.131	0.308	0.174	0.116	0.206	0.345	0.256	0.183
Lake Charles, LA	0.109	0.321	0.162	0.113	0.109	0.296	0.166	0.112
Los Angeles, CA	0.092	0.164	0.082	0.056	0.088	0.139	0.082	0.061
Louisville, KY	0.172	0.325	0.189	0.131	0.228	0.338	0.245	0.176
Memphis, TN	0.128	0.327	0.168	0.113	0.165	0.329	0.209	0.148
Miami, FL	0.093	0.297	0.173	0.126	0.108	0.289	0.202	0.153
Nashville, TN	0.114	0.398	0.211	0.143	0.172	0.450	0.310	0.222
New York, NY	0.094	0.207	0.115	0.080	0.075	0.158	0.091	0.065
Philadelphia, PA	0.145	0.269	0.143	0.097	0.177	0.265	0.175	0.124
Phoenix, AZ	0.144	0.249	0.139	0.086	0.194	0.261	0.190	0.131
Portland, OR	0.134	0.294	0.174	0.126	0.172	0.295	0.215	0.161
Richmond, VA	0.136	0.277	0.152	0.102	0.188	0.278	0.201	0.146
Sacramento, CA	0.141	0.303	0.160	0.105	0.191	0.307	0.208	0.146
St Louis, MO	0.159	0.226	0.123	0.083	0.171	0.211	0.144	0.103
Salt Lake City, UT	0.114	0.268	0.163	0.108	0.168	0.285	0.222	0.159
San Antonio, TX	0.192	0.240	0.149	0.110	0.223	0.247	0.186	0.140
San Diego, CA	0.110	0.176	0.108	0.078	0.099	0.143	0.097	0.070
San Francisco, CA	0.112	0.154	0.091	0.064	0.085	0.113	0.071	0.051
Tampa, FL	0.221	0.294	0.160	0.115	0.209	0.263	0.160	0.113
Tulsa, OK	0.167	0.301	0.164	0.111	0.209	0.307	0.208	0.146
Washington, DC	0.133	0.266	0.147	0.102	0.186	0.279	0.199	0.148

CONCLUSIONS

This project has been successful in obtaining information needed to reduce uncertainties in estimating atmospheric ozone impacts of 2,3,3,3-tetrafluoropropene. The available kinetic and mechanistic data for this compound are sufficient to derive an atmospheric reaction mechanism for this compound that can be used to estimate its atmospheric ozone impacts. However, the mechanism had uncertainties and estimates that needed to be tested, and experimental data were needed to establish the predictive capability of the mechanism before its predictions can be used as a basis for VOC exemption decisions. The experiments carried out for this project were successful in establishing the predictive capability of the mechanism developed for this compound, though some adjustments had to be made in order for the mechanism to simulate the data. These adjustments were well within the uncertainty of the estimates, so the mechanism can now be considered to be reasonably well established.

The evaluated mechanism predicted that the ozone impacts of 2,3,3,3-tetrafluoropropene, on a mass basis are essentially the same as those for ethane. The reactivities relative to ethane averaged 0.9±0.2 for all scenarios considered, and 1.0 ±0.1 for the MIR scenarios, i.e. well within the scenario-to-scenario variability of being the same. Note that all the scenarios considered are one-day simulations, and compounds that react in the atmosphere more slowly than ethane might have higher relatively higher ozone impacts in multi-day simulations. However, 2,3,3,3-tetrafluoropropene reacts somewhat more rapidly than ethane in the atmosphere, so if anything its ozone impacts relative to ethane are more likely to decrease in multi-day simulations. Therefore, if ethane is used as the standard to define "negligible" ozone impact for the purpose of determining VOC exemptions for ozone precursors, then 2,3,3,3-tetrafluoropropene should meet this standard.

The uncertain portion of the 2,3,3,3-tetrafluoropropene mechanism that had to be adjusted to yield satisfactory simulations of the chamber data concerned the nitrate yields in the reaction of NO with the initially formed $HOC_3F_4H_2OO\cdot$ peroxy radicals. The overall nitrate yield was previously estimated to be negligible (Carter, 2008b), and indeed this mechanism that gave best fits to the data in this study, so it was not modified as a result of this experimental study. However, the data for trans 1,3,3,3-tetrafluoropropene were best fit if an overall nitrate yield of ~5% was assumed (Carter, 2009b), suggesting that this should have been the case for 2,3,3,3-tetrafluoropropene as well. The fact that the best fit mechanisms suggest different nitrate yields for these tetrafluoropropenes suggest that the position of the fluorine atoms on the molecule has an effect on the overall nitrate yields in the photooxidation mechanism. Note, however, that these yields are derived indirectly based on modeling ozone reactivity, and not direct measurements of nitrate formation.

The near-explicit mechanism developed for this compound permits predictions of the gas-phase products formed in the atmospheric oxidations of 2,3,3,3-tetrafluoropropene. In the case of this compound the major products expected are formaldehyde, trifluoroacetyl fluoride, and the fluorinated hydroperoxides $CF_3CF(OH)CH_2OOH$ and $CF_3CF(OOH)CH_2OH$, which are expected to react primarily to form formaldehyde and trifluoroacetyl fluoride. The formaldehyde will be primarily oxidized to CO and CO_2, but the trifluoroacetyl fluoride is expected to be relatively stable in the gas phase, though it presumably will eventually hydrolyze in the environment to HF and trifluoroacetic acid. The mechanism developed in this work could be used for modeling the formation of these products.

Although this was outside the stated scope of this project, data were also obtained in this project concerning the effects of 2,3,3,3-tetrafluoropropene on atmospheric particle formation. The results indicated that the addition of this compound to atmospheric reactive organic gas surrogate - NO_x irradiations either had no effect on the mass or particles formed, or slightly reduced it. This indicates that

this compound does not form measurable amounts of secondary organic aerosol. This is as expected, since it is not predicted to form low volatility products. Furthermore, the products that it forms apparently do not also undergo significant heterogeneous reactions to form condensable compounds, at least under the relatively clean and dry conditions of these experiments.

REFERENCES

Atkinson, R. (1989): "Kinetics and Mechanisms of the Gas-Phase Reactions of the Hydroxyl Radical with Organic Compounds," J. Phys. Chem. Ref. Data, Monograph no 1.

Atkinson, R. (1991): "Kinetics and Mechanisms of the Gas-Phase Reactions of the NO_3 Radical with Organic Compounds," J. Phys. Chem. Ref. Data, 20, 459-507.

Atkinson, R. (1997): "Gas Phase Tropospheric Chemistry of Volatile Organic Compounds: 1. Alkanes and Alkenes," J. Phys. Chem. Ref. Data, 26, 215-290.

Baugues, K. (1990): "Preliminary Planning Information for Updating the Ozone Regulatory Impact Analysis Version of EKMA," Draft Document, Source Receptor Analysis Branch, Technical Support Division, U. S. Environmental Protection Agency, Research Triangle Park, NC, January.

CARB (1993): "Proposed Regulations for Low-Emission Vehicles and Clean Fuels -- Staff Report and Technical Support Document," California Air Resources Board, Sacramento, CA, August 13, 1990. See also Appendix VIII of "California Exhaust Emission Standards and Test Procedures for 1988 and Subsequent Model Passenger Cars, Light Duty Trucks and Medium Duty Vehicles," as last amended September 22, 1993. Incorporated by reference in Section 1960.

CARB (2000): "Initial Statement of Reasons for the Proposed Amendments to the Regulation for Reducing Volatile Organic Compound Emissions from Aerosol Coating Products and Proposed Tables of Maximum Incremental Reactivity (MIR) Values, and Proposed Amendments to Method 310, 'Determination of Volatile Organic Compounds in Consumer Products'," California Air Resources Board, Sacramento, CA, May 5.

CARB (2008): "Air Resources Board Reactivity Programs." Web page at http://www.arb.ca.gov/research/reactivity/reactivity.htm. Last updated June, 2008

Calvert, J. G., R. Atkinson, J. A. Kerr, S. Madronich, G. K. Moortgat, T. J. Wallington and G. Yarwood (2003): "The Mechanisms of Atmospheric Oxidation of Alkenes," Oxford University Press, New York,

Carter, W. P. L. (1994a): "Development of Ozone Reactivity Scales for Volatile Organic Compounds," J. Air & Waste Manage. Assoc., 44, 881-899.

Carter, W. P. L. (1994b): "Calculation of Reactivity Scales Using an Updated Carbon Bond IV Mechanism," Report Prepared for Systems Applications International Under Funding from the Auto/Oil Air Quality Improvement Research Program, April 12.

Carter, W. P. L. (2000a): "Documentation of the SAPRC-99 Chemical Mechanism for VOC Reactivity Assessment," Report to the California Air Resources Board, Contracts 92-329 and 95-308, May 8. Available at http://cert.ucr.edu/~carter/absts.htm#saprc99 and http://www.cert.ucr.edu/~carter/reactdat.htm.

Carter, W. P. L. (2000b): "Implementation of the SAPRC-99 Chemical Mechanism into the Models-3 Framework," Report to the United States Environmental Protection Agency, January 29. Available at http://www.cert.ucr.edu/~carter/absts.htm#s99mod3.

Carter, W. P. L. (2002): "Development of a Next Generation Environmental Chamber Facility for Chemical Mechanism and VOC Reactivity Research," Draft Research Plan and First Progress Report to the United States Environmental Protection Agency Cooperative Agreement CR 827331-01-0, January 3. Available at http://www.cert.ucr.edu/~carter/epacham.

Carter, W. P. L. (2004): "Evaluation of a Gas-Phase Atmospheric Reaction Mechanism for Low NO_x Conditions," Final Report to California Air Resources Board Contract No. 01-305, May 5. Available at http://www.cert.ucr.edu/~carter/absts.htm#lnoxrpt.

Carter, W. P. L. (2007): "Investigation of the Atmospheric Ozone Impacts of Methyl Iodide," Final Report to Arysta LifeScience Corporation, Contract UCR-07041867, July 31. Available at http://www.cert.ucr.edu/~carter/absts.htm#ch3irep.

Carter, W. P. L. (2008). "Estimation of the Ground-Level Atmospheric Ozone Formation Potential of 2,3,3,3-Tetrafluoropropene," Draft Report to Honeywell International Inc – Specialty Materials, June 23.

Carter, W. P. L. (2009a): "Development of the SAPRC-07 Chemical Mechanism and Updated Ozone Reactivity Scale," Revised final report to the California Air Resources Board Contract No. 03-318, March 20. Available at http://www.cert.ucr.edu/~carter/SAPRC.

Carter, W. P. L. (2009b). "Investigation of the Atmospheric Ozone Impacts of Trans 1,3,3,3-Tetra-fluoropropene," Final Report to Honeywell International Inc. Contract UCR-09010016, February 9. Available at http://www.cert.ucr.edu/~carter/absts.htm #ZEErept.

Carter, W. P. L. and R. Atkinson (1987): "An Experimental Study of Incremental Hydrocarbon Reactivity," Environ. Sci. Technol., 21, 670-679

Carter, W. P. L. and R. Atkinson (1989): "A Computer Modeling Study of Incremental Hydrocarbon Reactivity", Environ. Sci. Technol., 23, 864.

Carter, W. P .L., and Lurmann, F. W. (1991) Evaluation of a detailed gas-phase atmospheric reaction mechanism using environmental chamber data. Atmos. Environ. 25A:2771-2806.

Carter, W. P. L., J. A. Pierce, I. L. Malkina, D. Luo and W. D. Long (1993): "Environmental Chamber Studies of Maximum Incremental Reactivities of Volatile Organic Compounds," Report to Coordinating Research Council, Project No. ME-9, California Air Resources Board Contract No. A032-0692; South Coast Air Quality Management District Contract No. C91323, United States Environmental Protection Agency Cooperative Agreement No. CR-814396-01-0, University Corporation for Atmospheric Research Contract No. 59166, and Dow Corning Corporation. April 1. Available at http://www.cert.ucr.edu/~carter/absts.htm#rct1rept

Carter, W. P. L., D. Luo, I. L. Malkina, and D. Fitz (1995a): "The University of California, Riverside Environmental Chamber Data Base for Evaluating Oxidant Mechanism. Indoor Chamber Experiments through 1993," Report submitted to the U. S. Environmental Protection Agency, EPA/AREAL, Research Triangle Park, NC., March 20..

Carter, W. P. L., D. Luo, I. L. Malkina, and J. A. Pierce (1995b): "Environmental Chamber Studies of Atmospheric Reactivities of Volatile Organic Compounds. Effects of Varying ROG Surrogate and NO_x," Final report to Coordinating Research Council, Inc., Project ME-9, California Air Resources Board, Contract A032-0692, and South Coast Air Quality Management District, Contract C91323. March 24. Available at http://www.cert.ucr.edu/~carter/absts.htm#rct2rept.

Carter, W. P. L., J. H. Seinfeld, D. R. Fitz and G. S. Tonnesen (1999): "Development of a Next-Generation Environmental Chamber Facility for Chemical Mechanism and VOC Reactivity Evaluation," Research Proposal to the United States Environmental Protection Agency, February 22. (Available at http://www.cert.ucr.edu/~carter/epacham/proposal.htm.)

Carter, W. P. L. and I. L. Malkina (2005): "Evaluation of Atmospheric Impacts of Selected Coatings VOC Emissions," Final report to the California Air Resources Board Contract No. 00-333, March 15. Available at http://www.cert.ucr.edu/~carter/absts.htm#coatrpt.

Carter, W. P. L., D. R. Cocker III, D. R. Fitz, I. L. Malkina, K. Bumiller, C. G. Sauer, J. T. Pisano, C. Bufalino, and C. Song (2005a): "A New Environmental Chamber for Evaluation of Gas-Phase Chemical Mechanisms and Secondary Aerosol Formation", Atmos. Environ. 39 7768-7788.

Carter, W. P. L., I. L. Malkina, D. R. Cocker III, and C. Song (2005b): "Environmental Chamber Studies of VOC Species in Architectural Coatings and Mobile Source Emissions," Final Report to the South Coast Air Quality Management District Contract No. 03468, July 5. Available at http://www.cert.ucr.edu/~carter/absts.htm#scaqcham.

Carter, W. P. L. and I. L. Malkina (2007): "Investigation of the Atmospheric Impacts of Selected Pesticides," Final Report to the California Air Resources Board Contract 04-334, January 10. Available at http://www.cert.ucr.edu/~carter/absts.htm#pestrep.

Cocker, D. R., R. C. Flagan, and J. H. Seinfeld. (2001). "State-of-the-Art Chamber Facility for Studying Atmospheric Aerosol Chemistry," Environ. Sci. Technol. 35, 2594-2601.

Collins D. R., R. C. Flagan, and J. H. Seinfeld (2002). "Improved inversion of scanning DMA data," Aerosol Science Technology, 36, 2-9.

Dimitriades, B. (1999): "Scientific Basis of an Improved EPA Policy on Control of Organic Emissions for Ambient Ozone Reduction," J. Air & Waste Manage. Assoc. 49, 831-838

EPA (2005): "Interim Guidance on Control of Volatile Organic Compounds in Ozone State Implementation Plans," Federal Register, 70, 54046-54051, September 13.

Hurley, M.D., T.J. Wallington, M.S. Javadi, and O.J. Nielsen (2008): "Atmospheric chemistry of $CF_3CF{=}CH_2$: Products and mechanisms of Cl atom and OH radical initiated oxidation," Chemical Physics Letters 450, 263-267

IUPAC (2004a): IUPAC Subcommittee on Gas Kinetic Data Evaluation – Data Sheet PF1 Website: http://www.iupac-kinetic.ch.cam.ac.uk/. July 23.

IUPAC (2004b): IUPAC Subcommittee on Gas Kinetic Data Evaluation – Data Sheet PF3 Website: http://www.iupac-kinetic.ch.cam.ac.uk/. July 23.

IUPAC (2005): IUPAC Subcommittee on Gas Kinetic Data Evaluation – Data Sheet oFOx30 Website: http://www.iupac-kinetic.ch.cam.ac.uk/. March 29.

IUPAC (2006): "Evaluated Kinetic and Photochemical Data". IUPAC Subcommittee on Gas Kinetic Data Evaluation for Atmospheric Chemistry. Web Version. Available at http://www.iupac-kinetic.ch.cam.ac.uk. Latest data sheets dated June, 2006.

Johnson, G. M. (1983): "Factors Affecting Oxidant Formation in Sydney Air," in "The Urban Atmosphere -- Sydney, a Case Study." Eds. J. N. Carras and G. M. Johnson (CSIRO, Melbourne), pp. 393-408.

Nielsen, O.J., M.S. Javadi, M.P. Sulbaek Andersen, M.D. Hurley, T.J. Wallington, and R. Singh (2007): "Atmospheric chemistry of $CF_3CF=CH_2$: Kinetics and mechanisms of gas-phase reactions with Cl atoms, OH radicals, and O3," Chem. Phys. Lett. 439, 18-22

Orlando, J. J. and G. S. Tyndall (2003): "Gas phase UV absorption spectra for peracetic acid, and for acetic acid monomers and dimers," J. Photochem. Photobiol A, 157, 161-166.

RRWG (1999a): "VOC Reactivity Policy White Paper," Prepared by the Reactivity Research Work Group Policy Team, October 1. Available at http://www.narsto.org/section.src?SID=10.

Sellevåg, S. R.; Kelly, T.; Sidebottom, H.; Nielsen, C. J. (2004): "A study of the IR and UV-Vis absorption cross-sections, photolysis and OH-initiated oxidation of CF_3CHO and CF_3CH_2CHO," Phys. Chem. Chem. Phys. 6, 1243-1252.

Wallington, T. J. and Hurley, M. D. (1993): "Atmospheric chemistry of formyl fluoride: reaction with hydroxyl radicals," Environ. Sci. Technol., 27, 1448–1452.

Zafonte, L., P. L. Rieger, and J. R. Holmes (1977): "Nitrogen Dioxide Photolysis in the Los Angeles Atmosphere," Environ. Sci. Technol. 11, 483-487.

APPENDIX A. BASE MECHANISM LISTING

Table A-1. List of model species used in the base SAPRC-07 mechanism, including the VOC species used in the chamber and atmospheric reactivity simulations. The model species used for 2,3,3,3-tetrafluoropropene and its reaction products and intermediates are given in Table 2, above.

Name	Description
Constant Species.	
O2	Oxygen
M	Air
H2O	Water
H2	Hydrogen Molecules
HV	Light
Active Inorganic Species.	
O3	Ozone
NO	Nitric Oxide
NO2	Nitrogen Dioxide
NO3	Nitrate Radical
N2O5	Nitrogen Pentoxide
HONO	Nitrous Acid
HNO3	Nitric Acid
HNO4	Peroxynitric Acid
HO2H	Hydrogen Peroxide
CO	Carbon Monoxide
SO2	Sulfur Dioxide
H2	Hydrogen
Active Radical Species and Operators.	
OH	Hydroxyl Radicals
HO2	Hydroperoxide Radicals
MEO2	Methyl Peroxy Radicals
RO2C	Peroxy Radical Operator representing NO to NO_2 and NO_3 to NO_2 conversions, and the effects of peroxy radical reactions on acyl peroxy and other peroxy radicals.
RO2XC	Peroxy Radical Operator representing NO consumption (used in conjunction with organic nitrate formation), and the effects of peroxy radical reactions on NO_3, acyl peroxy radicals, and other peroxy radicals.
MECO3	Acetyl Peroxy Radicals
RCO3	Peroxy Propionyl and higher peroxy acyl Radicals
BZCO3	Peroxyacyl radical formed from Aromatic Aldehydes
MACO3	Peroxyacyl radicals formed from methacrolein and other acroleins.
Steady State Radical Species	
O3P	Ground State Oxygen Atoms
O1D	Excited Oxygen Atoms
TBUO	t-Butoxy Radicals
BZO	Phenoxy Radicals

Table A-1 (continued)

Name	Description
PAN and PAN Analogues	
PAN	Peroxy Acetyl Nitrate
PAN2	PPN and other higher alkyl PAN analogues
PBZN	PAN analogues formed from Aromatic Aldehydes
MAPAN	PAN analogue formed from Methacrolein
Explicit and Lumped Molecule Reactive Organic Product Species	
HCHO	Formaldehyde
CCHO	Acetaldehyde
RCHO	Lumped C3+ Aldehydes. Mechanism based on propionaldehyde
ACET	Acetone
MEK	Ketones and other non-aldehyde oxygenated products that react with OH radicals faster than 5 x 10^{-13} but slower than 5 x 10^{-12} cm^3 $molec^{-2}$ sec^{-1}. Mechanism based on methyl ethyl ketone.
MEOH	Methanol
HCOOH	Formic Acid
CCOOH	Acetic Acid. Also used for peroxyacetic acid.
RCOOH	Higher organic acids and peroxy acids. Mechanism based on propionic acid.
COOH	Methyl Hydroperoxide
ROOH	Lumped organic hydroperoxides with 2-4 carbons. Mechanism based n-propyl hydroperoxide.
R6OOH	Lumped organic hydroperoxides with 5 or more carbons (other than those formed following OH addition to aromatic rings, which are represented separately). Mechanism based on 3-hexyl hydroperoxide.
RAOOH	Organic hydroperoxides formed following OH addition to aromatic rings, which is represented separately because of their probable role in SOA formation. Mechanism based on two isomers expected to be formed in the m-xylene system.
GLY	Glyoxal
MGLY	Methyl Glyoxal
BACL	Biacetyl
CRES	Phenols and Cresols. Mechanism based on o-cresol.
NPHE	Nitrophenols
BALD	Aromatic aldehydes. Mechanism based on benzaldehyde
MACR	Methacrolein
MVK	Methyl Vinyl Ketone
IPRD	Lumped isoprene product species. Mechanism based on that of Carter and Atkinson (1996).
Aromatic unsaturated ring fragmentation products (see discussion of aromatic mechanisms)	
AFG1	Lumped photoreactive monounsaturated dicarbonyl aromatic fragmentation products that photolyze to form radicals.
AFG2	Lumped photoreactive monounsaturated dicarbonyl aromatic fragmentation products that photolyze to form non-radical products
AFG3	Lumped diunsaturatred dicarbonyl aromatic fragmentation product.

Table A-1 (continued)

Name	Description
Lumped Parameter Products	
PROD2	Ketones and other non-aldehyde oxygenated products that react with OH radicals faster than 5 x 10^{-12} cm^3 $molec^{-2}$ sec^{-1}. Mechanism based on $CH_3C(O)CH_2CH_2CH_2OH$, $CH_3C(O)$-$CH_2CH(CH_3)CH_2OH$, $CH_3CH_2C(O)CH_2CH_2CH(CH_3)OH$, $CH_3CH_2C(O)CH_2CH_2CH(OH)$-$CH_2CH_3$, and $CH_3CH_2CH_2CH(OH)CH_2$-$CH_2C(O)CH_2CH_3$ (PROD2-1 through 5), each weighed equally.
RNO3	Lumped Organic Nitrates. Mechanism based on $CH_3CH_2CH(CH_3)ONO_2$, $CH_3CH(OH)CH_2$-$CH_2CH_2ONO_2$, $CH_3CH_2CH(CH_3)CH(CH_3)ONO_2$, $CH_3CH_2CH_2CH_2CH_2CH(ONO_2)CH_2OH$, $CH_3CH_2C(CH_3)(ONO_2)CH_2CH(CH_3)CH_3$, and $CH_3CH_2CH_2CH_2CH_2CH_2CH_2CH(ONO_2)$-$CH_2CH_3$ (RNO3-1 through 6), each weighed equally.
Steady state operators used to represent radical or product formation in peroxy radical reactions.	
xHO2	Formation of HO_2 from alkoxy radicals formed in peroxy radical reactions with NO and NO_3 (100% yields) and RO_2 (50% yields)
xOH	As above, but for OH
xNO2	As above, but for NO_2
xMEO2	As above, but for MEO2
xMECO3	As above, but for MECO3
xRCO3	As above, but for RCO3
xMACO3	As above, but for MACO3
xTBUO	As above, but for TBUO
xCO	As above, but for CO
xHNO3	As above, but for HNO3
xHCHO	As above, but for HCHO
xCCHO	As above, but for CCHO
xRCHO	As above, but for RCHO
xACET	As above, but for ACET
xMEK	As above, but for MEK
xPROD2	As above, but for PROD2
xGLY	As above, but for GLY
xMGLY	As above, but for MGLY
xBACL	As above, but for BACL
xBALD	As above, but for BALD
xAFG1	As above, but for AFG1
xAFG2	As above, but for AFG2
xAFG3	As above, but for AFG3
xMACR	As above, but for MACR
xMVK	As above, but for MVK
xIPRD	As above, but for IPRD
xRNO3	As above, but for RNO3
xHCOOH	As above, but for HCOOH
xCCOOH	As above, but for CCOOH
xRCOOH	As above, but for RCOOH
zRNO3	Formation of RNO3 in the RO_2 + NO, reaction, or formation of corresponding non-nitrate products (represented by PROD2) formed from alkoxy radicals formed in RO_2 + NO_3 and (in 50% yields) RO_2 + RO_2 reactions.

Table A-1 (continued)

Name	Description
yROOH	Formation of ROOH following $RO_2 + HO_2$ reactions, or formation of H-shift disproportionation products (represented by MEK) in the $RO_2 + RCO_3$ and (in 50% yields) $RO_2 + RO_2$ reactions.
yR6OOH	As above, but with the $RO_2 + HO_2$ product represented by R6OOH and the H-shift products are represented by PROD2.
yRAOOH	As above, but with the $RO_2 + HO_2$ product represented by R6OOH
Non-Reacting Species	
CO2	Carbon Dioxide
SULF	Sulfates (SO_3 or H_2SO_4)
XC	Lost Carbon or carbon in unreactive products
XN	Lost Nitrogen or nitrogen in unreactive products
Primary Organics Represented explicitly	
CH4	Methane
ETHENE	Ethene
ISOPRENE	Isoprene
ACETYLEN	Acetylene
BENZENE	Benzene
ETHANE	Ethane (not part of the base mechanism, but used in atmospheric reactivity simulations)
Organics represented explicitly in the chamber simulations (not used in the atmospheric simulations)	
N-C4	n-Butane
N-C6	n-Hexane
N-C8	n-Octane
PROPENE	Propene
T-2-BUTE	trans-2-Butene
TOLUENE	Toluene
M-XYLENE	m-Xylene
Lumped model species used in the atmospheric reactivity simulations (not used in chamber simulations)	
ALK1	Alkanes and other non-aromatic compounds that react only with OH, and have kOH (OH radical rate constant) between 2 and 5 x 10^2 ppm^{-1} min^{-1}. (Primarily ethane)
ALK2	Alkanes and other non-aromatic compounds that react only with OH, and have kOH between 5 x 10^2 and 2.5 x 10^3 ppm^{-1} min^{-1}. (Primarily propane)
ALK3	Alkanes and other non-aromatic compounds that react only with OH, and have kOH between 2.5 x 10^3 and 5 x 10^3 ppm^{-1} min^{-1}.
ALK4	Alkanes and other non-aromatic compounds that react only with OH, and have kOH between 5 x 10^3 and 1 x 10^4 ppm^{-1} min^{-1}.
ALK5	Alkanes and other non-aromatic compounds that react only with OH, and have kOH greater than 1 x 10^4 ppm-1 min-1.
ARO1	Aromatics with kOH < $2x10^4$ ppm^{-1} min^{-1}.
ARO2	Aromatics with kOH > $2x10^4$ ppm^{-1} min^{-1}.
OLE1	Alkenes (other than ethene) with kOH < $7x10^4$ ppm^{-1} min^{-1}.
OLE2	Alkenes with kOH > $7x10^4$ ppm^{-1} min^{-1}.
TERP	Terpenes

Table A-2. Reactions and rate constants in the SAPRC-07 mechanism used in this work. See Carter (2009a) for documentation. The reactions used for 2,3,3,3-tetrafluoropropene are given in Table 3, above.

Label	Reaction and Products [a]	Rate Parameters [b] k(300)	A	Ea	B
Inorganic Reactions					
1	NO2 + HV = NO + O3P	Phot Set= NO2-06			
2	O3P + O2 + M = O3 + M	5.68e-34	5.68e-34	0.00	-2.60
3	O3P + O3 = #2 O2	8.34e-15	8.00e-12	4.09	
4	O3P + NO = NO2	1.64e-12	Falloff, F=0.60, N=1.00		
		0:	9.00e-32	0.00	-1.50
		inf:	3.00e-11	0.00	0.00
5	O3P + NO2 = NO + O2	1.03e-11	5.50e-12	-0.37	
6	O3P + NO2 = NO3	3.24e-12	Falloff, F=0.60, N=1.00		
		0:	2.50e-31	0.00	-1.80
		inf:	2.20e-11	0.00	-0.70
7	O3 + NO = NO2 + O2	2.02e-14	3.00e-12	2.98	
8	O3 + NO2 = O2 + NO3	3.72e-17	1.40e-13	4.91	
9	NO + NO3 = #2 NO2	2.60e-11	1.80e-11	-0.22	
10	NO + NO + O2 = #2 NO2	1.93e-38	3.30e-39	-1.05	
11	NO2 + NO3 = N2O5	1.24e-12	Falloff, F=0.35, N=1.33		
		0:	3.60e-30	0.00	-4.10
		inf:	1.90e-12	0.00	0.20
12	N2O5 = NO2 + NO3	5.69e-2	Falloff, F=0.35, N=1.33		
		0:	1.30e-3	21.86	-3.50
		inf:	9.70e+14	22.02	0.10
13	N2O5 + H2O = #2 HNO3	2.50e-22			
14	N2O5 + H2O + H2O = #2 HNO3 + H2O	1.80e-39			
	N2O5 + HV = NO3 + NO + O3P	(Slow)			
	N2O5 + HV = NO3 + NO2	(Slow)			
15	NO2 + NO3 = NO + NO2 + O2	6.75e-16	4.50e-14	2.50	
16	NO3 + HV = NO + O2	Phot Set= NO3NO-06			
17	NO3 + HV = NO2 + O3P	Phot Set= NO3NO2-6			
18	O3 + HV = O1D + O2	Phot Set= O3O1D-06			
19	O3 + HV = O3P + O2	Phot Set= O3O3P-06			
20	O1D + H2O = #2 OH	1.99e-10			
21	O1D + M = O3P + M	3.28e-11	2.38e-11	-0.19	
22	OH + NO = HONO	7.31e-12	Falloff, F=0.60, N=1.00		
		0:	7.00e-31	0.00	-2.60
		inf:	3.60e-11	0.00	-0.10
23	HONO + HV = OH + NO	Phot Set= HONO-06			
24	OH + HONO = H2O + NO2	5.95e-12	2.50e-12	-0.52	
25	OH + NO2 = HNO3	1.05e-11	Falloff, F=0.60, N=1.00		
		0:	1.80e-30	0.00	-3.00
		inf:	2.80e-11	0.00	0.00
26	OH + NO3 = HO2 + NO2	2.00e-11			

Table A-2 (continued)

Label	Reaction and Products [a]	Rate Parameters [b] k(300)	A	Ea	B
27	OH + HNO3 = H2O + NO3	1.51e-13	k = k0+k3M/(1+k3M/k2)		
		k0:	2.40e-14	-0.91	0.00
		k2:	2.70e-17	-4.37	0.00
		k3:	6.50e-34	-2.65	0.00
28	HNO3 + HV = OH + NO2	Phot Set= HNO3			
29	OH + CO = HO2 + CO2	2.28e-13	k = k1 + k2 [M]		
		k1:	1.44e-13	0.00	0.00
		k2:	3.43e-33	0.00	0.00
30	OH + O3 = HO2 + O2	7.41e-14	1.70e-12	1.87	
31	HO2 + NO = OH + NO2	8.85e-12	3.60e-12	-0.54	
32	HO2 + NO2 = HNO4	1.12e-12	Falloff, F=0.60, N=1.00		
		0:	2.00e-31	0.00	-3.40
		inf:	2.90e-12	0.00	-1.10
33	HNO4 = HO2 + NO2	1.07e-1	Falloff, F=0.60, N=1.00		
		0:	3.72e-5	21.16	-2.40
		inf:	5.42e+15	22.20	-2.30
34	HNO4 + HV = #.61 {HO2 + NO2} + #.39 {OH + NO3}	Phot Set= HNO4-06			
35	HNO4 + OH = H2O + NO2 + O2	4.61e-12	1.30e-12	-0.76	
36	HO2 + O3 = OH + #2 O2	2.05e-15	2.03e-16	-1.38	4.57
37	HO2 + HO2 = HO2H + O2	2.84e-12	k = k1 + k2 [M]		
		k1:	2.20e-13	-1.19	0.00
		k2:	1.90e-33	-1.95	0.00
38	HO2 + HO2 + H2O = HO2H + O2 + H2O	6.09e-30	k = k1 + k2 [M]		
		k1:	3.08e-34	-5.56	0.00
		k2:	2.66e-54	-6.32	0.00
39	NO3 + HO2 = #.8 {OH + NO2 + O2} + #.2 {HNO3 + O2}	4.00e-12			
40	NO3 + NO3 = #2 NO2 + O2	2.41e-16	8.50e-13	4.87	
41	HO2H + HV = #2 OH	Phot Set= H2O2			
42	HO2H + OH = HO2 + H2O	1.80e-12	1.80e-12	0.00	
43	OH + HO2 = H2O + O2	1.10e-10	4.80e-11	-0.50	
44	OH + SO2 = HO2 + SULF	9.49e-13	Falloff, F=0.60, N=1.00		
		0:	3.30e-31	0.00	-4.30
		inf:	1.60e-12	0.00	0.00
45	OH + H2 = HO2 + H2O	7.02e-15	7.70e-12	4.17	
<u>Methyl peroxy and methoxy reactions</u>					
BR01	MEO2 + NO = NO2 + HCHO + HO2	7.64e-12	2.30e-12	-0.72	
BR02	MEO2 + HO2 = COOH + O2	4.65e-12	3.46e-13	-1.55	0.36
BR03	MEO2 + HO2 = HCHO + O2 + H2O	4.50e-13	3.34e-14	-1.55	-3.53
BR04	MEO2 + NO3 = HCHO + HO2 + NO2	1.30e-12			
BR05	MEO2 + MEO2 = MEOH + HCHO + O2	2.16e-13	6.39e-14	-0.73	-1.80
BR06	MEO2 + MEO2 = #2 {HCHO + HO2}	1.31e-13	7.40e-13	1.03	
<u>Active Peroxy Radical Operators</u>					
BR07	RO2C + NO = NO2	9.23e-12	2.60e-12	-0.76	
BR08	RO2C + HO2 = HO2	7.63e-12	3.80e-13	-1.79	

Table A-2 (continued)

Label	Reaction and Products [a]	Rate Parameters [b] k(300)	A	Ea	B
BR09	RO2C + NO3 = NO2	2.30e-12			
BR10	RO2C + MEO2 = #.5 {RO2C + xHO2 + xHCHO + O2} + #.25 {HCHO + MEOH}	2.00e-13			
BR11	RO2C + RO2C =	3.50e-14			
BR12	RO2XC + NO = XN	Same k as rxn BR07			
BR13	RO2XC + HO2 = HO2	Same k as rxn BR08			
BR14	RO2XC + NO3 = NO2	Same k as rxn BR09			
BR15	RO2XC + MEO2 = #.5 {RO2C + xHO2 + xHCHO + O2} + #.25 {HCHO + MEOH}	Same k as rxn BR10			
BR16	RO2XC + RO2C =	Same k as rxn BR11			
BR17	RO2XC + RO2XC =	Same k as rxn BR11			
Reactions of Acyl Peroxy Radicals, PAN, and PAN analogues					
BR18	MECO3 + NO2 = PAN	9.37e-12	Falloff, F=0.30, N=1.41		
		0:	2.70e-28	0.00	-7.10
		inf:	1.21e-11	0.00	-0.90
BR19	PAN = MECO3 + NO2	6.27e-4	Falloff, F=0.30, N=1.41		
		0:	4.90e-3	24.05	0.00
		inf:	4.00e+16	27.03	0.00
BR20	PAN + HV = #.6 {MECO3 + NO2} + #.4 {MEO2 + CO2 + NO3}	Phot Set= PAN			
BR21	MECO3 + NO = MEO2 + CO2 + NO2	1.97e-11	7.50e-12	-0.58	
BR22	MECO3 + HO2 = CCOOH + #.7 O2 + #.3 O3	1.36e-11	5.20e-13	-1.95	
BR23	MECO3 + NO3 = MEO2 + CO2 + NO2 + O2	Same k as rxn BR09			
BR24	MECO3 + MEO2 = #.9 {CCOOH + HCHO + O2} + #.1 {HCHO + HO2 + MEO2 + CO2}	1.06e-11	2.00e-12	-0.99	
BR25	MECO3 + RO2C = CCOOH	1.56e-11	4.40e-13	-2.13	
BR26	MECO3 + RO2XC = CCOOH	Same k as rxn BR25			
BR27	MECO3 + MECO3 = #2 {MEO2 + CO2} + O2	1.54e-11	2.90e-12	-0.99	
BR28	RCO3 + NO2 = PAN2	1.21e-11	1.21e-11	0.00	-1.07
BR29	PAN2 = RCO3 + NO2	5.48e-4	8.30e+16	27.70	
BR30	RCO3 + NO = NO2 + RO2C + xHO2 + yROOH + xCCHO + CO2	2.08e-11	6.70e-12	-0.68	
BR31	RCO3 + HO2 = RCOOH + #.75 O2 + #.25 O3	Same k as rxn BR22			
BR32	RCO3 + NO3 = NO2 + RO2C + xHO2 + yROOH + xCCHO + CO2 + O2	Same k as rxn BR09			
BR33	RCO3 + MEO2 = RCOOH + HCHO + O2	Same k as rxn BR24			
BR34	RCO3 + RO2C = RCOOH + O2	Same k as rxn BR25			
BR35	RCO3 + RO2XC = RCOOH + O2	Same k as rxn BR25			
BR36	RCO3 + MECO3 = #2 CO2 + MEO2 + RO2C + xHO2 + yROOH + xCCHO + O2	Same k as rxn BR27			
BR37	RCO3 + RCO3 = #2 {RO2C + xHO2 + xCCHO + yROOH + CO2}	Same k as rxn BR27			
BR38	BZCO3 + NO2 = PBZN	1.37e-11			
BR39	PBZN = BZCO3 + NO2	4.27e-4	7.90e+16	27.82	
BR40	BZCO3 + NO = NO2 + CO2 + BZO + RO2C	Same k as rxn BR30			

Table A-2 (continued)

Label	Reaction and Products [a]	Rate Parameters [b] k(300)	A	Ea	B
BR41	BZCO3 + HO2 = RCOOH + #.75 O2 + #.25 O3 + #4 XC	Same k as rxn BR22			
BR42	BZCO3 + NO3 = NO2 + CO2 + BZO + RO2C + O2	Same k as rxn BR09			
BR43	BZCO3 + MEO2 = RCOOH + HCHO + O2 + #4 XC	Same k as rxn BR24			
BR44	BZCO3 + RO2C = RCOOH + O2 + #4 XC	Same k as rxn BR25			
BR45	BZCO3 + RO2XC = RCOOH + O2 + #4 XC	Same k as rxn BR25			
BR46	BZCO3 + MECO3 = #2 CO2 + MEO2 + BZO + RO2C	Same k as rxn BR27			
BR47	BZCO3 + RCO3 = #2 CO2 + RO2C + xHO2 + yROOH + xCCHO + BZO + RO2C	Same k as rxn BR27			
BR48	BZCO3 + BZCO3 = #2 {BZO + RO2C + CO2}	Same k as rxn BR27			
BR49	MACO3 + NO2 = MAPAN	Same k as rxn BR28			
BR50	MAPAN = MACO3 + NO2	4.79e-4	1.60e+16	26.80	
BR51	MACO3 + NO = NO2 + CO2 + HCHO + MECO3	Same k as rxn BR30			
BR52	MACO3 + HO2 = RCOOH + #.75 O2 + #.25 O3 + XC	Same k as rxn BR22			
BR53	MACO3 + NO3 = NO2 + CO2 + HCHO + MECO3 + O2	Same k as rxn BR09			
BR54	MACO3 + MEO2 = RCOOH + HCHO + XC + O2	Same k as rxn BR24			
BR55	MACO3 + RO2C = RCOOH + XC	Same k as rxn BR25			
BR56	MACO3 + RO2XC = RCOOH + O2 + XC	Same k as rxn BR25			
BR57	MACO3 + MECO3 = #2 CO2 + MEO2 + HCHO + MECO3 + O2	Same k as rxn BR27			
BR58	MACO3 + RCO3 = HCHO + MECO3 + RO2C + xHO2 + yROOH + xCCHO + #2 CO2	Same k as rxn BR27			
BR59	MACO3 + BZCO3 = HCHO + MECO3 + BZO + RO2C + #2 CO2	Same k as rxn BR27			
BR60	MACO3 + MACO3 = #2 {HCHO + MECO3 + CO2}	Same k as rxn BR27			
Other Organic Radical Species					
BR61	TBUO + NO2 = RNO3 + #-2 XC	2.40e-11			
BR62	TBUO = ACET + MEO2	1.18e+3	7.50e+14	16.20	
BR63	BZO + NO2 = NPHE	3.79e-11	2.30e-11	-0.30	
BR64	BZO + HO2 = CRES + #-1 XC	Same k as rxn BR08			
BR65	BZO = CRES + RO2C + xHO2 + #-1 XC	1.00e-3			
Steady-State Peroxy Radical operators (for formation of inorganic and radical products) [c]					
RO01	xHO2 = HO2	k is variable parameter: RO2RO			
RO02	xHO2 =	k is variable parameter: RO2XRO			
RO03	xOH = OH	k is variable parameter: RO2RO			
RO04	xOH =	k is variable parameter: RO2XRO			
RO05	xNO2 = NO2	k is variable parameter: RO2RO			
RO06	xNO2 = XN	k is variable parameter: RO2XRO			
RO07	xMEO2 = MEO2	k is variable parameter: RO2RO			
RO08	xMEO2 = XC	k is variable parameter: RO2XRO			
RO09	xMECO3 = MECO3	k is variable parameter: RO2RO			
RO10	xMECO3 = #2 XC	k is variable parameter: RO2XRO			
RO11	xRCO3 = RCO3	k is variable parameter: RO2RO			
RO12	xRCO3 = #3 XC	k is variable parameter: RO2XRO			
RO13	xMACO3 = MACO3	k is variable parameter: RO2RO			

Table A-2 (continued)

Label	Reaction and Products [a]	Rate Parameters [b] k(300)	A	Ea	B
RO14	xMACO3 = #4 XC	k is variable parameter: RO2XRO			
RO15	xTBUO = TBUO	k is variable parameter: RO2RO			
RO16	xTBUO = #4 XC	k is variable parameter: RO2XRO			
RO17	xCO = CO	k is variable parameter: RO2RO			
RO18	xCO = XC	k is variable parameter: RO2XRO			
RO19	xHNO3 = HNO3	k is variable parameter: RO2RO			
RO20	xHNO3 = XN	k is variable parameter: RO2XRO			
Explicit and Lumped Molecule Organic Products					
BP01	HCHO + HV = #2 HO2 + CO	Phot Set= HCHOR-06			
BP02	HCHO + HV = H2 + CO	Phot Set= HCHOM-06			
BP03	HCHO + OH = HO2 + CO + H2O	8.47e-12	5.40e-12	-0.27	
BP07	HCHO + NO3 = HNO3 + HO2 + CO	6.06e-16	2.00e-12	4.83	
BP08	CCHO + OH = MECO3 + H2O	1.49e-11	4.40e-12	-0.73	
BP09	CCHO + HV = CO + HO2 + MEO2	Phot Set= CCHO_R			
BP10	CCHO + NO3 = HNO3 + MECO3	2.84e-15	1.40e-12	3.70	
BP11	RCHO + OH = #.965 RCO3 + #.035 {RO2C + xHO2 + xCO + xCCHO + yROOH}	1.97e-11	5.10e-12	-0.80	
BP12	RCHO + HV = RO2C + xHO2 + yROOH + xCCHO + CO + HO2	Phot Set= C2CHO			
BP13	RCHO + NO3 = HNO3 + RCO3	6.74e-15	1.40e-12	3.18	
BP14	ACET + OH = RO2C + xMECO3 + xHCHO + yROOH	1.91e-13	4.56e-14	-0.85	3.65
BP15	ACET + HV = #.62 MECO3 + #1.38 MEO2 + #.38 CO	Phot Set= ACET-06, qy= 0.5			
BP16	MEK + OH = #.967 RO2C + #.039 {RO2XC + zRNO3} + #.376 xHO2 + #.51 xMECO3 + #.074 xRCO3 + #.088 xHCHO + #.504 xCCHO + #.376 xRCHO + yROOH + #.3 XC	1.20e-12	1.30e-12	0.05	2.00
BP17	MEK + HV = MECO3 + RO2C + xHO2 + xCCHO + yROOH	Phot Set= MEK-06, qy= 0.175			
BP18	MEOH + OH = HCHO + HO2	9.02e-13	2.85e-12	0.69	
BP19	HCOOH + OH = HO2 + CO2	4.50e-13			
BP20	CCOOH + OH = #.509 MEO2 + #.491 RO2C + #.509 CO2 + #.491 xHO2 + #.491 xMGLY + #.491 yROOH + #-0.491 XC	7.26e-13	4.20e-14	-1.70	
BP21	RCOOH + OH = RO2C + #.08 CO2 + xHO2 + #.063 CO2 + #.142 xCCHO + #.4 xRCHO + #.457 xBACL + yROOH + #-0.455 XC	1.20e-12			
BP22	COOH + OH = H2O + #.3 {HCHO + OH} + #.7 MEO2	7.40e-12	3.80e-12	-0.40	
BP23	COOH + HV = HCHO + HO2 + OH	Phot Set= COOH			
BP24	ROOH + OH = #.744 OH + #.251 RO2C + #.004 RO2XC + #.004 zRNO3 + #.744 RCHO + #.239 xHO2 + #.012 xOH + #.012 xHCHO + #.012 xCCHO + #.205 xRCHO + #.034 xPROD2 + #.256 yROOH + #-0.115 XC	2.50e-11			
BP25	ROOH + HV = RCHO + HO2 + OH	Phot Set= COOH			

Table A-2 (continued)

Label	Reaction and Products [a]	Rate Parameters [b] k(300)	A	Ea	B
BP26	R6OOH + OH = #.84 OH + #.222 RO2C + #.029 RO2XC + #.029 zRNO3 + #.84 PROD2 + #.09 xHO2 + #.041 xOH + #.02 xCCHO + #.075 xRCHO + #.084 xPROD2 + #.16 yROOH + #.02 XC	5.60e-11			
BP27	R6OOH + HV = OH + #.142 HO2 + #.782 RO2C + #.077 RO2XC + #.077 zRNO3 + #.085 RCHO + #.142 PROD2 + #.782 xHO2 + #.026 xCCHO + #.058 xRCHO + #.698 xPROD2 + #.858 yR6OOH + #.017 XC	Phot Set= COOH			
BP28	RAOOH + OH = #.139 OH + #.148 HO2 + #.589 RO2C + #.124 RO2XC + #.124 zRNO3 + #.074 PROD2 + #.147 MGLY + #.139 IPRD + #.565 xHO2 + #.024 xOH + #.448 xRCHO + #.026 xGLY + #.030 xMEK + #.252 xMGLY + #.073 xAFG1 + #.073 xAFG2 + #.713 yR6OOH + #2.674 XC	1.41e-10			
BP29	RAOOH + HV = OH + HO2 + #.5 {GLY + MGLY + AFG1 + AFG2} + #.5 XC	Phot Set= COOH			
BP30	GLY + HV = #2 {CO + HO2}	Phot Set= GLY-07R			
BP31	GLY + HV = HCHO + CO	Phot Set= GLY-07M			
BP32	GLY + OH = #.63 HO2 + #1.26 CO + #.37 RCO3 + #-.37 XC	1.10e-11			
BP33	GLY + NO3 = HNO3 + #.63 HO2 + #1.26 CO + #.37 RCO3 + #-.37 XC	1.02e-15	2.80e-12	4.72	
BP34	MGLY + HV = HO2 + CO + MECO3	Phot Set= MGLY-06			
BP35	MGLY + OH = CO + MECO3	1.50e-11			
BP36	MGLY + NO3 = HNO3 + CO + MECO3	2.53e-15	1.40e-12	3.77	
BP37	BACL + HV = #2 MECO3	Phot Set= BACL-07			
BP38	CRES + OH = #.2 BZO + #.8 {RO2C + xHO2 + yR6OOH} + #.25 xMGLY + #5.05 XC	4.03e-11	1.70e-12	-1.89	
BP39	CRES + NO3 = HNO3 + BZO + XC	1.40e-11			
BP40	NPHE + OH = BZO + XN	3.50e-12			
BP41	NPHE + HV = HONO + #6 XC	Phot Set= NO2-06, qy= 1.5e-3			
BP42	NPHE + HV = #6 XC + XN	Phot Set= NO2-06, qy= 1.5e-2			
BP43	BALD + OH = BZCO3	1.20e-11			
BP44	BALD + HV = #7 XC	Phot Set= BALD-06, qy= 0.06			
BP45	BALD + NO3 = HNO3 + BZCO3	2.73e-15	1.34e-12	3.70	

Table A-2 (continued)

Label	Reaction and Products [a]	Rate Parameters [b] k(300)	A	Ea	B
Lumped Unsaturated Aromatic Ring-Opening Products					
BP46	AFG1 + OH = #.217 MACO3 + #.723 RO2C + #.060 {RO2XC + zRNO3} + #.060 zRNO3 + #.521 xHO2 + #.201 xMECO3 + #.334 xCO + #.407 xRCHO + #.129 xMEK + #.107 xGLY + #.267 xMGLY + #.783 yR6OOH + #-.076 XC	7.40e-11			
BP47	AFG1 + O3 = #.826 OH + #.522 HO2 + #.652 RO2C + #.522 CO + #.174 CO2 + #.432 GLY + #.568 MGLY + #.652 xRCO3 + #.652 xHCHO + #.652 yR6OOH + #-.872 XC	9.66e-18			
BP48	AFG1 + HV = #1.023 HO2 + #.173 MEO2 + #.305 MECO3 + #.500 MACO3 + #.695 CO + #.195 GLY + #.305 MGLY + #.217 XC	Phot Set= AFG1			
BP49	AFG2 + OH = #.217 MACO3 + #.723 RO2C + #.060 {RO2XC + zRNO3} + #.060 zRNO3 + #.521 xHO2 + #.201 xMECO3 + #.334 xCO + #.407 xRCHO + #.129 xMEK + #.107 xGLY + #.267 xMGLY + #.783 yR6OOH + #-.076 XC	7.40e-11			
BP50	AFG2 + O3 = #.826 OH + #.522 HO2 + #.652 RO2C + #.522 CO + #.174 CO2 + #.432 GLY + #.568 MGLY + #.652 xRCO3 + #.652 xHCHO + #.652 yR6OOH + #-.872 XC	9.66e-18			
BP51	AFG2 + HV = PROD2 + #-1 XC	Phot Set= AFG1			
BP52	AFG3 + OH = #.206 MACO3 + #.733 RO2C + #.117 {RO2XC + zRNO3} + #.117 zRNO3 + #.561 xHO2 + #.117 xMECO3 + #.114 xCO + #.274 xGLY + #.153 xMGLY + #.019 xBACL + #.195 xAFG1 + #.195 xAFG2 + #.231 xIPRD + #.794 yR6OOH + #.236 XC	9.35e-11			
BP53	AFG3 + O3 = #.471 OH + #.554 HO2 + #.013 MECO3 + #.258 RO2C + #.007 {RO2XC + zRNO3} + #.007 zRNO3 + #.580 CO + #.190 CO2 + #.366 GLY + #.184 MGLY + #.350 AFG1 + #.350 AFG2 + #.139 AFG3 + #.003 MACR + #.004 MVK + #.003 IPRD + #.095 xHO2 + #.163 xRCO3 + #.163 xHCHO + #.095 xMGLY + #.264 yR6OOH + #-.617 XC	1.43e-17			
BP54	MACR + OH = #.5 MACO3 + #.5 {RO2C + xHO2} + #.416 xCO + #.084 xHCHO + #.416 xMEK + #.084 xMGLY + #.5 yROOH + #-0.416 XC	2.84e-11	8.00e-12	-0.76	
BP55	MACR + O3 = #.208 OH + #.108 HO2 + #.1 RO2C + #.45 CO + #.117 CO2 + #.1 HCHO + #.9 MGLY + #.333 HCOOH + #.1 xRCO3 + #.1 xHCHO + #.1 yROOH + #-0.1 XC	1.28e-18	1.40e-15	4.17	
BP56	MACR + NO3 = #.5 {MACO3 + RO2C + HNO3 + xHO2 + xCO} + #.5 yROOH + #1.5 XC + #.5 XN	3.54e-15	1.50e-12	3.61	
BP57	MACR + O3P = RCHO + XC	6.34e-12			

Table A-2 (continued)

Label	Reaction and Products [a]	Rate Parameters [b] k(300)	A	Ea	B
BP58	MACR + HV = #.33 OH + #.67 HO2 + #.34 MECO3 + #.33 MACO3 + #.33 RO2C + #.67 CO + #.34 HCHO + #.33 xMECO3 + #.33 xHCHO + #.33 yROOH	Phot Set= MACR-06			
BP59	MVK + OH = #.975 RO2C + #.025 {RO2XC + zRNO3} + #.3 xHO2 + #.675 xMECO3 + #.3 xHCHO + #.675 xRCHO + #.3 xMGLY + yROOH + #-0.725 XC	1.99e-11	2.60e-12	-1.21	
BP60	MVK + O3 = #.164 OH + #.064 HO2 + #.05 {RO2C + xHO2} + #.475 CO + #.124 CO2 + #.05 HCHO + #.95 MGLY + #.351 HCOOH + #.05 xRCO3 + #.05 xHCHO + #.05 yROOH + #-0.05 XC	5.36e-18	8.50e-16	3.02	
BP61	MVK + NO3 = #4 XC + XN		(Slow)		
BP62	MVK + O3P = #.45 RCHO + #.55 MEK + #.45 XC	4.32e-12			
BP63	MVK + HV = #.4 MEO2 + #.6 CO + #.6 PROD2 + #.4 MACO3 + #-2.2 XC	Phot Set= MVK-06			
BP64	IPRD + OH = #.289 MACO3 + #.67 {RO2C + xHO2} + #.041 {RO2XC + zRNO3} + #.336 xCO + #.055 xHCHO + #.129 xCCHO + #.013 xRCHO + #.15 xMEK + #.332 xPROD2 + #.15 xGLY + #.174 xMGLY + #-0.504 XC + #.711 yR6OOH	6.19e-11			
BP65	IPRD + O3 = #.285 OH + #.4 HO2 + #.048 {RO2C + xRCO3} + #.498 CO + #.14 CO2 + #.124 HCHO + #.21 MEK + #.023 GLY + #.742 MGLY + #.1 HCOOH + #.372 RCOOH + #.047 xCCHO + #.001 xHCHO + #.048 yR6OOH + #-.329 XC	4.18e-18			
BP66	IPRD + NO3 = #.15 {MACO3 + HNO3} + #.799 {RO2C + xHO2} + #.051 {RO2XC + zRNO3} + #.572 xCO + #.227 xHCHO + #.218 xRCHO + #.008 xMGLY + #.572 xRNO3 + #.85 yR6OOH + #.278 XN + #-.815 XC	1.00e-13			
BP67	IPRD + HV = #1.233 HO2 + #.467 MECO3 + #.3 RCO3 + #1.233 CO + #.3 HCHO + #.467 CCHO + #.233 MEK + #-.233 XC	Phot Set= MACR-06			
<u>Lumped Parameter Organic Products</u>					
BP68	PROD2 + OH = #.472 HO2 + #.473 RO2C + #.070 RO2XC + #.070 zRNO3 + #.002 HCHO + #.001 CCHO + #.143 RCHO + #.329 PROD2 + #.379 xHO2 + #.029 xMECO3 + #.049 xRCO3 + #.211 xHCHO + #.083 xCCHO + #.402 xRCHO + #.115 xMEK + #.007 xPROD2 + #.528 yR6OOH + #.883 XC	1.55e-11			
BP69	PROD2 + HV = #.400 MECO3 + #.600 RCO3 + #1.590 RO2C + #.086 RO2XC + #.086 zRNO3 + #.914 xHO2 + #.303 xHCHO + #.163 xCCHO + #.780 xRCHO + yR6OOH + #-.085 XC	Phot Set= MEK-06, qy= 4.86e-3			

Table A-2 (continued)

Label	Reaction and Products [a]	Rate Parameters [b] k(300)	A	Ea	B
BP70	RNO3 + OH = #.019 NO2 + #.189 HO2 + #.976 RO2C + #.175 RO2XC + #.175 zRNO3 + #.001 RCHO + #.010 MEK + #.007 PROD2 + #.189 RNO3 + #.312 xNO2 + #.305 xHO2 + #.011 xHCHO + #.428 xCCHO + #.036 xRCHO + #.004 xACET + #.170 xMEK + #.030 xPROD2 + #.305 xRNO3 + #.792 yR6OOH + #.175 XN + #.054 XC	7.20e-12			
BP71	RNO3 + HV = NO2 + #.344 HO2 + #.721 RO2C + #.102 RO2XC + #.102 zRNO3 + #.074 HCHO + #.214 CCHO + #.074 RCHO + #.124 MEK + #.190 PROD2 + #.554 xHO2 + #.061 xHCHO + #.230 xCCHO + #.063 xRCHO + #.008 xACET + #.083 xMEK + #.261 xPROD2 + #.656 yR6OOH + #.396 XC	Phot Set= IC3ONO2			

Steady-State Peroxy Radical operators (for formation of organic product species formed in peroxy + NO reactions) [c]

PO01	xHCHO = HCHO	k is variable parameter: RO2RO
PO02	xHCHO = XC	k is variable parameter: RO2XRO
PO03	xCCHO = CCHO	k is variable parameter: RO2RO
PO04	xCCHO = #2 XC	k is variable parameter: RO2XRO
PO05	xRCHO = RCHO	k is variable parameter: RO2RO
PO06	xRCHO = #3 XC	k is variable parameter: RO2XRO
PO07	xACET = ACET	k is variable parameter: RO2RO
PO08	xACET = #3 XC	k is variable parameter: RO2XRO
PO09	xMEK = MEK	k is variable parameter: RO2RO
PO10	xMEK = #4 XC	k is variable parameter: RO2XRO
PO11	xPROD2 = PROD2	k is variable parameter: RO2RO
PO12	xPROD2 = #6 XC	k is variable parameter: RO2XRO
PO13	xGLY = GLY	k is variable parameter: RO2RO
PO14	xGLY = #2 XC	k is variable parameter: RO2XRO
PO15	xMGLY = MGLY	k is variable parameter: RO2RO
PO16	xMGLY = #3 XC	k is variable parameter: RO2XRO
PO17	xBACL = BACL	k is variable parameter: RO2RO
PO18	xBACL = #4 XC	k is variable parameter: RO2XRO
PO19	xBALD = BALD	k is variable parameter: RO2RO
PO20	xBALD = #7 XC	k is variable parameter: RO2XRO
PO21	xAFG1 = AFG1	k is variable parameter: RO2RO
PO22	xAFG1 = #5 XC	k is variable parameter: RO2XRO
PO23	xAFG2 = AFG2	k is variable parameter: RO2RO
PO24	xAFG2 = #5 XC	k is variable parameter: RO2XRO
PO25	xAFG3 = AFG3	k is variable parameter: RO2RO
PO26	xAFG3 = #7 XC	k is variable parameter: RO2XRO
PO27	xMACR = MACR	k is variable parameter: RO2RO
PO28	xMACR = #4 XC	k is variable parameter: RO2XRO
PO29	xMVK = MVK	k is variable parameter: RO2RO
PO30	xMVK = #4 XC	k is variable parameter: RO2XRO
PO31	xIPRD = IPRD	k is variable parameter: RO2RO
PO32	xIPRD = #5 XC	k is variable parameter: RO2XRO

Table A-2 (continued)

Label	Reaction and Products [a]	Rate Parameters [b] k(300)	A	Ea	B
PO33	xRNO3 = RNO3	k is variable parameter: RO2RO			
PO34	xRNO3 = #6 XC + XN	k is variable parameter: RO2XRO			
PO35	xHCOOH = HCOOH	k is variable parameter: RO2RO			
PO36	xHCOOH = XC	k is variable parameter: RO2XRO			
PO37	xCCOOH = CCOOH	k is variable parameter: RO2RO			
PO38	xCCOOH = #2 XC	k is variable parameter: RO2XRO			
PO39	xRCOOH = RCOOH	k is variable parameter: RO2RO			
PO40	xRCOOH = #3 XC	k is variable parameter: RO2XRO			
Steady-State Peroxy Radical operators (for formation of organic nitrates formed in peroxy + NO reactions) [d]					
PO41	zRNO3 = RNO3 + #-1 XN	k is variable parameter: RO2NO			
PO42	zRNO3 = PROD2 + HO2	k is variable parameter: RO22NN			
PO43	zRNO3 = #6 XC	k is variable parameter: RO2XRO			
Steady-State Peroxy Radical operators (for formation of hydroperoxides formed in peroxy + HO_2 reactions) [e]					
PO44	yROOH = ROOH + #-3 XC	k is variable parameter: RO2HO2			
PO45	yROOH = MEK + #-4 XC	k is variable parameter: RO2RO2M			
PO46	yROOH =	k is variable parameter: RO2RO			
PO47	yR6OOH = R6OOH + #-6 XC	k is variable parameter: RO2HO2			
PO48	yR6OOH = PROD2 + #-6 XC	k is variable parameter: RO2RO2M			
PO49	yR6OOH =	k is variable parameter: RO2RO			
PO50	yRAOOH = RAOOH + #-8 XC	k is variable parameter: RO2HO2			
PO51	yRAOOH = PROD2 + #-6 XC	k is variable parameter: RO2RO2M			
PO52	yRAOOH =	k is variable parameter: RO2RO			
Explicitly Represented Primary Organics					
BE01	CH4 + OH = H2O + MEO2	6.62e-15	1.85e-12	3.36	
BE02	ETHENE + OH = RO2C + xHO2 + #1.61 xHCHO + #.195 xCCHO + yROOH	8.15e-12	Falloff, F=0.60, N=1.00		
		0:	1.00e-28	0.00	-4.50
		inf:	8.80e-12	0.00	-0.85
BE03	ETHENE + O3 = #.16 OH + #.16 HO2 + #.51 CO + #.12 CO2 + HCHO + #.37 HCOOH	1.68e-18	9.14e-15	5.13	
BE04	ETHENE + NO3 = RO2C + xHO2 + xRCHO + yROOH + #-1 XC + XN	2.24e-16	3.30e-12	5.72	2.00
BE05	ETHENE + O3P = #.8 HO2 + #.51 MEO2 + #.29 RO2C + #.51 CO + #.1 CCHO + #.29 xHO2 + #.278 xCO + #.278 xHCHO + #.012 xGLY + #.29 yROOH + #.2 XC	7.43e-13	1.07e-11	1.59	
BE06	ISOPRENE + OH = #.986 RO2C + #.093 {RO2XC + zRNO3} + #.907 xHO2 + #.624 xHCHO + #.23 xMACR + #.32 xMVK + #.357 xIPRD + yR6OOH + #-0.167 XC	9.96e-11	2.54e-11	-0.81	
BE07	ISOPRENE + O3 = #.266 OH + #.066 HO2 + #.192 RO2C + #.008 {RO2XC + zRNO3} + #.275 CO + #.122 CO2 + #.4 HCHO + #.1 PROD2 + #.39 MACR + #.16 MVK + #.15 IPRD + #.204 HCOOH + #.192 {xMACO3 + xHCHO} + #.2 yR6OOH + #-0.559 XC	1.34e-17	7.86e-15	3.80	

Table A-2 (continued)

Label	Reaction and Products [a]	Rate Parameters [b] k(300)	A	Ea	B
BE08	ISOPRENE + NO3 = #.936 RO2C + #.064 {RO2XC + zRNO3} + #.749 xHO2 + #.187 xNO2 + #.936 xIPRD + yR6OOH + #-0.064 XC + #.813 XN	6.81e-13	3.03e-12	0.89	
BE09	ISOPRENE + O3P = #.25 MEO2 + #.24 RO2C + #.01 {RO2XC + zRNO3} + #.75 PROD2 + #.24 xMACO3 + #.24 xHCHO + #.25 yR6OOH + #-1.01 XC	3.50e-11			
BE10	ACETYLEN + OH = #.7 OH + #.3 HO2 + #.3 CO + #.7 GLY + #.3 HCOOH	7.56e-13	Falloff, F=0.60, N=1.00		
BE11	ACETYLEN + O3 = #.5 OH + #1.5 HO2 + #1.5 CO + #.5 CO2	1.16e-20	1.00e-14	8.15	
BE12	BENZENE + OH = #.116 OH + #.29 {RO2C + xHO2} + #.024 {RO2XC + zRNO3} + #.57 {HO2 + CRES} + #.116 AFG3 + #.290 xGLY + #.029 xAFG1 + #.261 xAFG2 + #.314 yRAOOH + #-.976 XC	1.22e-12	2.33e-12	0.38	
	Reactions of Compounds represented explicitly in the chamber simulations				
CH05	N-C4 + OH = #1.334 RO2C + #.079 RO2XC + #.079 zRNO3 + #.921 xHO2 + #.632 xCCHO + #.120 xRCHO + #.485 xMEK + yROOH + #-.038 XC	2.38e-12	1.63e-12	-0.23	
CH07	N-C6 + OH = #1.562 RO2C + #.225 RO2XC + #.225 zRNO3 + #.775 xHO2 + #.011 xCCHO + #.113 xRCHO + #.688 xPROD2 + yR6OOH + #.161 XC	5.25e-12	7.62e-12	0.22	
CH09	N-C8 + OH = #1.432 RO2C + #.354 RO2XC + #.354 zRNO3 + #.646 xHO2 + #.024 xRCHO + #.622 xPROD2 + yR6OOH + #2.072 XC	8.16e-12	2.45e-12	-0.72	
CH11	PROPENE + OH = #.984 RO2C + #.016 RO2XC + #.016 zRNO3 + #.984 xHO2 + #.984 xHCHO + #.984 xCCHO + yROOH + #-.048 XC	2.60e-11	4.85e-12	-1.00	
CH12	PROPENE + O3 = #.350 OH + #.165 HO2 + #.355 MEO2 + #.525 CO + #.215 CO2 + #.500 HCHO + #.500 CCHO + #.185 HCOOH + #.075 CCOOH + #.070 XC	1.05e-17	5.51e-15	3.73	
CH13	PROPENE + NO3 = #.949 RO2C + #.051 RO2XC + #.051 zRNO3 + #.949 xHO2 + yROOH + #2.694 XC + XN	9.73e-15	4.59e-13	2.30	
CH14	PROPENE + O3P = #.450 RCHO + #.550 MEK + #-.550 XC	4.01e-12	1.02e-11	0.56	
CH16	T-2-BUTE + OH = #.965 RO2C + #.035 RO2XC + #.035 zRNO3 + #.965 xHO2 + #1.930 xCCHO + yROOH + #-.070 XC	6.32e-11	1.01e-11	-1.09	
CH17	T-2-BUTE + O3 = #.540 OH + #.170 HO2 + #.710 MEO2 + #.540 CO + #.310 CO2 + CCHO + #.150 CCOOH + #.140 XC	1.95e-16	6.64e-15	2.10	
CH18	T-2-BUTE + NO3 = #.920 RO2C + #.080 RO2XC + #.080 zRNO3 + #.705 xNO2 + #.215 xHO2 + #1.410 xCCHO + #.215 xRNO3 + yROOH + #-.590 XC + #.080 XN	3.93e-13	1.10e-13	-0.76	
CH19	T-2-BUTE + O3P = MEK	1.99e-11	1.09e-11	-0.36	

Table A-2 (continued)

Label	Reaction and Products [a]	Rate Parameters [b] k(300)	A	Ea	B
CH21	TOLUENE + OH = #.312 {OH + AFG3} + #.181 {HO2 + CRES} + #.454 {RO2C + xHO2} + #.054 {RO2XC +zRNO3} + #.238 xGLY + #.151 xMGLY + #.065 xBALD + #.195 xAFG1 + #.195 xAFG2 + #.073 yR6OOH + #.435 yRAOOH + #-.109 XC	5.58e-12	1.81e-12	-0.67	
CH23	M-XYLENE + OH = #.239 {OH + AFG3} + #.159 {HO2 + CRES} + #.52 {RO2C +xHO2} + #.082 {RO2XC + zRNO3} + #.100 xGLY + #.380 xMGLY + #.041 xBALD + #.336 xAFG1 + #.144 xAFG2 + #.047 yR6OOH + #.555 yRAOOH+ #.695 XC	2.31e-11			
Reactions of Ethane used in its Atmospheric Reactivity Simulations					
C201	ETHANE + OH = RO2C + xHO2 + xCCHO + yROOH	2.54E-13	1.34E-12	0.992	2.0
Reactions of Lumped Species used in Atmospheric Reactivity Simulations					
BL01	ALK1 + OH = RO2C + xHO2 + xCCHO + yROOH	2.54e-13	1.34e-12	0.99	
BL02	ALK2 + OH = #.965 RO2C + #.035 {RO2XC + zRNO3} + #.965 xHO2 + #.261 xRCHO + #.704 xACET + yROOH + #-.105 XC	1.11e-12	1.49e-12	0.17	
BL03	ALK3 + OH = #1.253 RO2C + #.07 {RO2XC + zRNO3} + #.694 xHO2 + #.236 xTBUO + #.026 xHCHO + #.445 xCCHO + #.122 xRCHO + #.024 xACET + #.332 xMEK + yROOH + #-.046 XC	2.31e-12	1.51e-12	-0.25	
BL04	ALK4 + OH = #1.773 RO2C + #.144 {RO2XC + zRNO3} + #.834 xHO2 + #.011 xMEO2 + #.011 xMECO3 + #.002 xCO + #.030 xHCHO + #.454 xCCHO + #.242 xRCHO + #.442 xACET + #.110 xMEK + #.128 xPROD2 + yR6OOH + #-.097 XC	4.26e-12	3.67e-12	-0.09	
BL05	ALK5 + OH = #1.597 RO2C + #.348 {RO2XC + zRNO3} + #.652 xHO2 + #.037 xHCHO + #.099 xCCHO + #.199 xRCHO + #.066 xACET + #.080 xMEK + #.425 xPROD2 + yR6OOH + #2.012 XC	9.22e-12	2.65e-12	-0.74	
BL06	OLE1 + OH = #1.138 RO2C + #.095 {RO2XC + zRNO3} + #.904 xHO2 + #.001 xMEO2 + #.700 xHCHO + #.301 xCCHO + #.470 xRCHO + #.005 xACET + #.119 xPROD2 + #.026 xMACR + #.008 xMVK + #.006 xIPRD + yROOH + #.822 XC	3.29e-11	6.18e-12	-1.00	
BL07	OLE1 + O3 = #.193 OH + #.116 HO2 + #.104 MEO2 + #.063 RO2C + #.004 {RO2XC + zRNO3} + #.368 CO + #.125 CO2 + #.500 HCHO + #.147 CCHO + #.353 RCHO + #.006 MEK + #.189 PROD2 + #.185 HCOOH + #.022 CCOOH + #.112 RCOOH + #.040 xHO2 + #.007 xCCHO + #.031 xRCHO + #.002 xACET + #.044 yR6OOH + #.69 XC	1.09e-17	3.15e-15	3.38	
BL08	OLE1 + NO3 = #1.312 RO2C + #.176 {RO2XC + zRNO3} + #.824 xHO2 + #.009 xCCHO + #.002 xRCHO + #.024 xACET + #.546 xRNO3 + yR6OOH + #.454 XN + #.572 XC	1.44e-14	4.73e-13	2.08	

Table A-2 (continued)

Label	Reaction and Products [a]	Rate Parameters [b] k(300)	A	Ea	B
BL09	OLE1 + O3P = #.450 RCHO + #.437 MEK + #.113 PROD2 + #1.224 XC	5.02e-12	1.49e-11	0.65	
BL10	OLE2 + OH = #.966 RO2C + #.086 {RO2XC + zRNO3} + #.914 xHO2 + #.209 xHCHO + #.787 xCCHO + #.483 xRCHO + #.136 xACET + #.076 xMEK + #.021 xPROD2 + #.027 xMACR + #.002 xMVK + #.037 xIPRD + yR6OOH + #.113 XC	6.41e-11	1.26e-11	-0.97	
BL11	OLE2 + O3 = #.421 OH + #.093 HO2 + #.290 MEO2 + #.199 RO2C + #.003 {RO2XC + zRNO3} + #.296 CO + #.162 CO2 + #.152 HCHO + #.426 CCHO + #.316 RCHO + #.048 ACET + #.031 MEK + #.042 PROD2 + #.028 MACR + #.021 MVK + #.033 HCOOH + #.061 CCOOH + #.222 RCOOH + #.039 xHO2 + #.147 xMECO3 + #.007 xRCO3 + #.108 xHCHO + #.066 xCCHO + #.019 xRCHO + #.196 yR6OOH + #.133 XC	1.24e-16	8.15e-15	2.49	
BL12	OLE2 + NO3 = #1.185 RO2C + #.136 {RO2XC + zRNO3} + #.409 xNO2 + #.423 xHO2 + #.033 xMEO2 + #.074 xHCHO + #.546 xCCHO + #.153 xRCHO + #.110 xACET + #.002 xMEK + #.026 xMVK + #.007 xIPRD + #.322 xRNO3 + yR6OOH + #.270 XN + #.117 XC	7.70e-13	2.15e-13	-0.76	
BL13	OLE2 + O3P = #.014 HO2 + #.013 RO2C + #.074 RCHO + #.709 MEK + #.203 PROD2 + #.007 xHO2 + #.007 xMACO3 + #.006 xCO + #.006 xMACR + #.014 yR6OOH + #.666 XC	2.06e-11	1.43e-11	-0.22	
BL14	ARO1 + OH = #.283 OH + #.166 HO2 + #.483 RO2C + #.068 {RO2XC + zRNO3} + #.166 CRES + #.283 AFG3 + #.483 xHO2 + #.217 xGLY + #.138 xMGLY + #.049 xBALD + #.079 xPROD2 + #.164 xAFG1 + #.192 xAFG2 + #.150 yR6OOH + #.402 yRAOOH+ #.004 XC	6.18e-12			
BL15	ARO2 + OH = #.199 OH + #.108 HO2 + #.582 RO2C + #.111 RO2XC + #.111 zRNO3 + #.108 CRES + #.199 AFG3 + #.582 xHO2 + #.111 xGLY + #.291 xMGLY + #.104 xBACL + #.033 xBALD + #.042 xPROD2 + #.223 xAFG1 + #.211 xAFG2 + #.074 xAFG3 + #.090 yR6OOH + #.603 yRAOOH+ #1.503 XC	2.20e-11			
BL16	TERP + OH = #1.147 RO2C + #.2 {RO2XC + zRNO3} + #.759 xHO2 + #.042 xRCO3 + #.002 xCO + #.264 xHCHO + #.533 xRCHO + #.036 xACET + #.005 xMEK + #.255 xPROD2 + #.009 xMGLY + #.014 xBACL + #.002 xMVK + #.001 xIPRD + yR6OOH + #5.055 XC	7.98e-11	1.87e-11	-0.86	

Table A-2 (continued)

Label	Reaction and Products [a]	Rate Parameters [b] k(300)	A	Ea	B
BL17	TERP + O3 = #.585 OH + #.052 HO2 + #.875 RO2C + #.203 RO2XC + #.203 zRNO3 + #.166 CO + #.045 CO2 + #.079 HCHO + #.004 MEK + #.409 PROD2 + #.107 HCOOH + #.043 RCOOH + #.067 xHO2 + #.126 xMECO3 + #.149 xRCO3 + #.019 xCO + #.150 xHCHO + #.220 xRCHO + #.165 xACET + #.001 xGLY + #.002 xMGLY + #.055 xBACL + #.001 xMACR + #.001 xIPRD + #.545 yR6OOH + #3.526 XC	6.99e-17	1.02e-15	1.60	
BL18	TERP + NO3 = #1.508 RO2C + #.397 RO2XC + #.397 zRNO3 + #.422 xNO2 + #.162 xHO2 + #.019 xRCO3 + #.010 xCO + #.017 xHCHO + #.001 xCCHO + #.509 xRCHO + #.174 xACET + #.001 xMGLY + #.003 xMACR + #.001 xMVK + #.002 xIPRD + #.163 xRNO3 + yR6OOH + #4.476 XC + #.415 XN	6.53e-12	1.28e-12	-0.97	
BL19	TERP + O3P = #.147 RCHO + #.853 PROD2 + #4.441 XC	3.71e-11			

[a] Format of reaction listing: "=" separates reactants from products; "*#number*" indicates stoichiometric coefficient, "*#coefficient* {*product list*}" means that the stoichiometric coefficient is applied to all the products listed.

[b] Except as indicated, the rate constants are given by $k(T) = A \cdot (T/300)^B \cdot e^{-Ea/RT}$, where the units of k and A are cm^3 $molec^{-1}$ s^{-1}, Ea are kcal mol^{-1}, T is ^oK, and R=0.0019872 kcal mol^{-1} deg^{-1}. If A, Ea, and B are not given the rate constants are assumed to be temperature independent. The following special rate constant expressions are used:

Phot Set = *name*: The absorption cross sections and (if applicable) quantum yields for the photolysis reaction are given by Carter (2009). Here, "*name*" indicates the photolysis set used. If a "qy=*number*" notation is given, the number given is the overall quantum yield, which is assumed to be wavelength independent. Photolysis rates used in chamber and ambient simulations are given in Table A-3.

Falloff: The rate constant as a function of temperature and pressure is calculated using $k(T,M) = \{k0(T)\cdot[M]/[1 + k0(T)\cdot[M]/kinf(T)]\}\cdot F^Z$, where $Z = \{1 + [\log10\{k0(T)\cdot[M])/kinf(T)\}/N]^2\}^{-1}$, [M] is the total pressure in molecules cm^{-3}, F and N are as indicated on the table, and the temperature dependences of k0 and kinf are as indicated on the table.

k = k0+k3M(1+k3M/k2): The rate constant as a function of temperature and pressure is calculated using $k(T,M) = k0(T) + k3(T)\cdot[M] \cdot(1 + k3(T)\cdot[M]/k2(T))$, where [M] is the total bath gas (air) concentration in molecules cm-3, and the temperature dependences for k0, k2 and k3 are as indicated on the table.

k = k1 + k2 [M]: The rate constant as a function of temperature and pressure is calculated using $k(T,M) = k1(T) + k2(T)\cdot[M]$, where [M] is the total bath gas (air) concentration in molecules cm-3, and the temperature dependences for k1, and k2 are as indicated on the table.

Same K as Rxn xx: Uses the same rate constant as the reaction in the base mechanism with the same label.

k is variable parameter *name*: The rate constant is calculated using variable parameters that are calculated using concentrations of various species. See Footnotes [c], [d], and [e], below.

[c] The xPROD chemical operator species are used to represent the formation of radicals and products from alkoxy radicals formed in the reactions of peroxy radicals with NO, NO_3, and other peroxy

Table A-2 (continued)

radicals. These products are not formed when peroxy radicals react with HO_2 and acyl peroxy radicals, since those reactions are assumed not form alkoxy radicals, but instead form hydroperoxides or H-shift disproportion products that are represented by separate yROOH chemical operator species, discussed in a separate footnote. The reactions of peroxy radicals with other peroxy radicals are assumed to form alkoxy radicals 50% of the time, so the products from alkoxy radical reactions are represented as being formed in 50% yields in these reactions. The consumption and products formed from these species can be represented in several ways. The most straightforward method is to include a reaction for each of the types of peroxy radical reactions, as follows:

xPROD + NO → NO + PROD
xPROD + HO2 → HO2
xPROD + NO3 → NO3 + PROD
xPROD + MECO3 → MECO3 (& similar reactions for RCO3, BZCO3, and MACO3)
xPROD + RO2C → RO2C + 1/2 PROD (& a similar reaction for RO2XC)

where "PROD" represents the product species for the operator (e.g, HO2 for xHO2). The rate constants for these reactions should be the same as the rate constant for the corresponding reactions of RO2C or RO2XC. This is a somewhat cumbersome method because it requires 9 reactions for each of the many xPROD species. An alternative method, implemented in this table, uses the coefficient "RO2RO" to determine the rate of formation of the product species and "RO2XRO" to represent processes where the product is not formed. These are calculated as follows, where the k(RO2+..)'s refer to the rate constants for the reactions of RO2C or RO2XC with the indicated reactant.

RO2RO = k(RO2+NO)[NO] + k(RO2+NO3)[NO3] + 0.5 k(RO2+MEO2)[MEO2] +
0.5 k(RO2+RO2){[RO2C]+[RO2XC])

RO2XRO = k(RO2+HO2)[HO2] + k(RO2+MECO3){[MECO3]+[RCO3]+[BZCO3]+
[MACO3]) + 0.5 k(RO2+MEO2)[MEO2] + 0.5 k(RO2+RO2){[RO2C]+ [RO2XC])

The steady state approximation must be used for these operators when this representation is used, and the operators must not be allowed to be diluted or transported.

[d] The zRNO3 chemical operator species is used to represent the formation organic nitrates formed when peroxy radicals react with NO, or formation of of radicals and products from alkoxy radicals formed in the reactions of peroxy radicals with NO_3 and other peroxy radicals. These products are not formed when peroxy radicals react with HO_2 and acyl peroxy radicals, since those reactions are assumed not form organic nitrates or alkoxy radicals, but instead form hydroperoxides or H-shift disproportion products that are represented by separate yROOH chemical operator species, discussed in a separate footnote. At present the mechanism has only one zRNO3 operator to correspond to the single lumped organic nitrate model species, but other such operators can be added if it is desired to have separate organic nitrate model species, such as, for example, those to represent semi-volatile organic nitrates that may contribute to SOA. In the case of zRNO3, the products resulting if alkoxy radicals are formed in the RCO3 or RO2 reactions would depend on reactant and individual radicals, and are approximated by PROD2 and HO2 (as might occur following the reaction of a peroxy radical with O2 to form HO2 and a ketone species). As with the xPROD species, the consumption and products formed from these species can be represented in several ways, with the most straightforward method being to include a reaction for each of the types of peroxy radical reactions, as follows:

zRNO3 + NO → NO + RNO3
zRNO3 + HO2 → HO2
zRNO3 + NO3 → NO3 + PROD2 + HO2
zRNO3 + MECO3 → MECO3 (& similar reactions for RCO3, BZCO3, and MACO3)
zRNO3 + RO2C → RO2C + 1/2 {PROD2 + HO2} (& a similar reaction for RO2XC)

Table A-2 (continued)

The rate constants for these reactions should be the same as the rate constant for the corresponding reactions of RO2C or RO2XC. As with xPROD, an alternative method, requiring fewer reactions, is implemented in this table. In this case, the coefficient "RO2NO" is used to determine the rate of formation of organic nitrates, "RO22NN" is used to determine the rate of formation of the alkoxy radical products, and "RO2XRO" is used to represent processes where these products are is not formed, and is the same as used for xPROD. These are calculated as follows, where the k(RO2+..)'s refer to the rate constants for the reactions of RO2C or RO2XC with the indicated reactant.

RO2NO = k(RO2+NO)[NO]

RO22NN = k(RO2+NO3)[NO3] + 0.5 k(RO2+MEO2)[MEO2] + 0.5 k(RO2+RO2){[RO2C]+ [RO2XC])

RO2XRO = k(RO2+HO2)[HO2] + k(RO2+MECO3){[MECO3]+[RCO3]+[BZCO3]+ [MACO3]) + 0.5 k(RO2+MEO2)[MEO2] + 0.5 k(RO2+RO2){[RO2C]+ [RO2XC]) (same as used for xPROD)

The steady state approximation must be used for these operators when this representation is used, and the operators must not be allowed to be diluted or transported.

[e] The yROOH chemical operator species is used to represent the formation of organic hydroperoxides formed with peroxy radicals react with HO_2, or of H-shift disproportionation products formed when peroxy radicals react with acyl peroxy radicals or (in 50% yields) with other peroxy radicals. Note that the products formed when peroxy radicals react to form alkoxy radicals or organic nitrates (in the NO reaction) are represented using separate xPROD or zRNO3 species, and together these three types of operators represent all the products and radicals formed. Separate such yROOH species are used to represent formation of hydroperoxides or H-shift disproportion products in different molecular weight ranges or volatilities, and more can be added as needed for appropriate predictions of SOA formation. The hydroperoxide formed in the HO2 reaction is represented by either ROOH, R6OOH, or RAOOH, and the H-shift disproportion products are represented by either MEK (for yROOH) or PROD2 (for the others). As with the xPROD and zRNO3 species, the consumption and products formed from these species can be represented in several ways, with the most straightforward method being to include a reaction for each of the types of peroxy radical reactions, as follows for yROOH (the reactions for the other two are analogous).

yROOH + NO → NO

yROOH + HO2 → HO2 + ROOH

yROOH + NO3 → NO3

yROOH + MECO3 → MECO3 + MEK (& similar reactions for RCO3, BZCO3, and MACO3)

yROOH + RO2C → RO2C + 1/2 MEK (& a similar reaction for RO2XC)

The rate constants for these reactions should be the same as the rate constant for the corresponding reactions of RO2C or RO2XC. As with the other operators, an alternative method, requiring fewer reactions, is implemented in this table. In this case, the coefficient "RO2HO2" is used to determine the rate of formation of organic hydroperoxides, "RO2RO2M" to determine the rate of formation of H-shift disproportion products, and "RO2RO" is used to represent processes where these products are is not formed. Note that the latter is the same as the coefficient that is used to represent the formation products from the xPROD species. These are calculated as follows, where the k(RO2+..)'s refer to the rate constants for the reactions of RO2C or RO2XC with the indicated reactant.

RO2HO2 = k(RO2+HO2)[HO2]

RO2RO2M = k(RO2+MECO3){[MECO3]+[RCO3]+[BZCO3]+ [MACO3]) + 0.5 k(RO2+MEO2)[MEO2] + 0.5 k(RO2+RO2){[RO2C]+ [RO2XC])

Table A-2 (continued)

RO2RO = k(RO2+NO)[NO] + k(RO2+NO3)[NO3] + 0.5 k(RO2+MEO2)[MEO2] + 0.5 k(RO2+RO2){[RO2C]+[RO2XC])

The steady state approximation must be used for these operators when this representation is used, and the operators must not be allowed to be diluted or transported.

Table A-3. Summary of photolysis rates used in chamber and ambient simulations.

Phot File	Chamber [a]	Photolysis rates (min-1) Ambient simulations (as function of solar zenith angle) [b] Z=0	Z=10	Z=20	Z=30	Z=40	Z=50	Z=60	Z=70	Z=78	Z=86
Base Mechanism [c]											
NO2-06	0.115	0.723	0.718	0.702	0.676	0.631	0.560	0.430	0.253	0.093	0.005
NO3NO-06	2.44e-4	1.91e+0	1.91e+0	1.90e+0	1.89e+0	1.87e+0	1.82e+0	1.65e+0	1.37e+0	9.15e-1	4.85e-1
NO3NO2-6	4.83e-2	1.54e+1	1.54e+1	1.53e+1	1.52e+1	1.49e+1	1.44e+1	1.29e+1	1.03e+1	6.50e+0	2.80e+0
O3O1D-06	1.83e-4	3.06e-3	2.96e-3	2.68e-3	2.24e-3	1.67e-3	1.06e-3	4.91e-4	1.33e-4	2.01e-5	3.66e-7
O3O3P-06	4.84e-4	3.66e-2	3.66e-2	3.62e-2	3.57e-2	3.48e-2	3.32e-2	2.95e-2	2.37e-2	1.57e-2	8.36e-3
HONO-06	2.81e-2	1.14e-1	1.13e-1	1.10e-1	1.06e-1	9.78e-2	8.54e-2	6.38e-2	3.55e-2	1.18e-2	4.32e-4
HNO3	4.42e-6	5.40e-5	5.28e-5	4.91e-5	4.31e-5	3.49e-5	2.50e-5	1.40e-5	4.99e-6	9.91e-7	2.29e-8
HNO4-06	6.66e-5	5.42e-4	5.32e-4	5.01e-4	4.52e-4	3.81e-4	2.90e-4	1.77e-4	7.28e-5	1.70e-5	4.56e-7
H2O2	9.00e-5	5.64e-4	5.56e-4	5.29e-4	4.86e-4	4.21e-4	3.33e-4	2.14e-4	9.43e-5	2.35e-5	6.64e-7
PAN	7.17e-6	6.12e-5	6.00e-5	5.65e-5	5.08e-5	4.26e-5	3.22e-5	1.95e-5	7.90e-6	1.81e-6	4.80e-8
HCHOR-06	2.53e-4	2.76e-3	2.72e-3	2.59e-3	2.36e-3	2.03e-3	1.58e-3	9.85e-4	4.05e-4	9.08e-5	2.35e-6
HCHOM-06	6.12e-4	3.12e-3	3.08e-3	2.97e-3	2.77e-3	2.47e-3	2.02e-3	1.37e-3	6.41e-4	1.69e-4	5.00e-6
CCHO_R	2.53e-5	4.16e-4	4.06e-4	3.75e-4	3.27e-4	2.60e-4	1.81e-4	9.50e-5	2.99e-5	4.86e-6	8.30e-8
C2CHO	1.05e-4	1.40e-3	1.37e-3	1.28e-3	1.14e-3	9.29e-4	6.74e-4	3.80e-4	1.36e-4	2.62e-5	5.79e-7
ACET-06	3.85e-6	6.47e-5	6.28e-5	5.69e-5	4.78e-5	3.60e-5	2.32e-5	1.10e-5	3.05e-6	4.50e-7	7.35e-9
MEK-06	6.96e-5	9.66e-4	9.45e-4	8.80e-4	7.78e-4	6.33e-4	4.56e-4	2.54e-4	8.86e-5	1.66e-5	3.53e-7
COOH	7.11e-5	3.94e-4	3.89e-4	3.71e-4	3.42e-4	2.99e-4	2.40e-4	1.58e-4	7.21e-5	1.89e-5	5.51e-7
GLY-07R	9.60e-4	9.06e-3	9.00e-3	8.78e-3	8.44e-3	7.86e-3	6.97e-3	5.39e-3	3.29e-3	1.35e-3	1.31e-4
GLY-07M	4.40e-4	3.18e-3	3.14e-3	3.00e-3	2.78e-3	2.44e-3	1.98e-3	1.33e-3	6.41e-4	1.91e-4	8.80e-6
MGLY-06	1.02e-3	1.56e-2	1.56e-2	1.52e-2	1.47e-2	1.38e-2	1.24e-2	9.83e-3	6.27e-3	2.72e-3	2.87e-4
BACL-07	2.06e-3	2.67e-2	2.66e-2	2.61e-2	2.54e-2	2.40e-2	2.18e-2	1.75e-2	1.12e-2	4.81e-3	4.67e-4
BALD-06	1.32e-2	5.10e-2	5.05e-2	4.88e-2	4.61e-2	4.17e-2	3.52e-2	2.49e-2	1.26e-2	3.71e-3	1.17e-4
AFG1	6.82e-2	3.87e-1	3.83e-1	3.70e-1	3.50e-1	3.17e-1	2.69e-1	1.94e-1	1.04e-1	3.51e-2	1.99e-3
MACR-06	3.43e-5	1.97e-4	1.94e-4	1.86e-4	1.72e-4	1.51e-4	1.21e-4	7.98e-5	3.64e-5	9.42e-6	2.74e-7
MVK-06	1.32e-5	7.50e-5	7.40e-5	7.07e-5	6.54e-5	5.73e-5	4.60e-5	3.02e-5	1.37e-5	3.51e-6	1.01e-7
IC3ONO2	1.82e-5	2.35e-4	2.30e-4	2.15e-4	1.91e-4	1.57e-4	1.15e-4	6.57e-5	2.41e-5	4.80e-6	1.11e-7

[a] Photolysis rates for a chamber experiment with blacklight light source. The chamber photolysis rates are for the experiments carried out for this project.

[b] See Carter (1994) for documentation of solar actinic fluxes used in the atmospheric reactivity calculations.

[c] Calculated using absorption coefficients and cross sections given by Carter (2009)